

Stability of monolayers and bilayers in a copolymer-homopolymer blend model

Yves van Gennip*, Mark A. Peletier*

October 26, 2018

Abstract

We study the stability of layered structures in a variational model for diblock copolymer-homopolymer blends with respect to perturbations of their interfaces. The main step consists of calculating the first and second derivatives of a sharp-interface Ohta-Kawasaki energy for straight mono- and bilayers and determining the latter's sign. By developing the interface perturbations in a Fourier series we fully characterise the stability of the structures in terms of the energy parameters. Both for the monolayer and for the bilayer there exist parameter regions where these structures are unstable. For strong repulsive interaction between the monomer types in the diblock copolymer the bilayer is always stable with respect to interface perturbations, irrespective of the domain size. The monolayer is only stable for small domain size.

In the course of our computations we also give a Green's function for the Laplacian on a two-dimensional periodic strip.

Keywords: block copolymers, copolymer-homopolymer blends, pattern formation, variational model, partial localisation, Green's function for Laplacian on a strip

Mathematics Subject Classification (2000): 49N99, 82D60

1 Introduction

1.1 Localised and partially localised patterns

Localised patterns are observed in a wide variety of systems, including experimental systems such as the Belusov-Zabotinsky reaction [55], nonlinear optics [48, 46], vertically shaken granular media [52, 50], and Bose-Einstein condensates [47], and also in idealised systems such as the Swift-Hohenberg equation [11, 44, 45, 49] or networks of reacting cells [29]. More recently objects have been observed that are only *partially* localised: structures in two dimensions, for instance, that are 'thin' in one spatial direction and 'long' in the other. Such *partially localised patterns* have been observed in Nonlinear Schrödinger equations [13, 5, 1, 2, 3], Gierer-Meinhardt-type systems [14], and even in scalar nonlinear elliptic equations [26, 27, 25]. In addition, the membrane that surrounds each living cell, for instance, is such a structure [23, 7, 34].

In this paper we study an example of *energy-driven* partial localisation, arising in the study of mixtures of *diblock copolymers* with *homopolymers*. Such mixtures feature two opposing forces: a repelling force between different monomer types favours separation into homogeneous phases, while covalent bonds between some of the repelling monomers impose an upper limit on the separation length. As a result a wide variety of patterns are observed (both in physical and in numerical experiments), ranging from spheres [22, 33, 53, 57], cylinders [21], dumbbells [32], helices [19], 'labyrinths' and 'sponges' [24, 20, 32], 'ball-of-thread' [24], layered structures [21, 22, 32, 57], and many more.

*Dept. of Mathematics and Computer Science, Technische Universiteit Eindhoven, PO Box 513, 5600 MB Eindhoven, The Netherlands (e-mail: y.v.gennip@tue.nl, m.a.peletier@tue.nl)

Our focus is on *layered patterns*, consisting of two or more parallel layers of roughly uniform thickness. In each layer the composition is dominated by one of the polymer types, and in the separation into layers one can recognise a phase separation phenomenon triggered by the repelling forces between polymer types. In addition to their interest as particular patterns in copolymer-homopolymer blends, such layered structures are examples of energy-driven partial localisation.

The main goal of this article is to understand the (in)stability of such layered structures in this simple model of copolymer-homopolymer blends.

1.2 Diblock copolymers and blends

Diblock copolymers are linear polymer molecules that consist of two parts (blocks) called the U-part and the V-part in this paper, with corresponding volume fractions given by the functions u and v . Each part contains monomers of a single type only, U or V. As described above, the interaction between the two types of monomers is the net result of two opposing influences. On the one hand the U- and V-parts repel each other, leading to a tendency of the U- and V-phases to separate; on the other hand the U- and V-parts are chemically bonded together in a single diblock copolymer molecule, forcing both parts to remain close to each other. As a result of these two types of interaction, the separation between the U- and V-phases is restricted to length scales of the order of the molecule size.

We consider systems that contain, in addition to the diblock copolymers, some species of *homopolymer*, that we call the 0-phase. A homopolymer is made up of a single type of monomers, here named 0. The system therefore contains three phases, and because of an assumption of incompressibility we can use the functions u and v to describe the distributions of the three phases.

In [8] the following energy is derived:

$$\mathcal{F}(u, v) = \begin{cases} c_0 \int_{S_L} |\nabla(u+v)| + c_u \int_{S_L} |\nabla u| + c_v \int_{S_L} |\nabla v| + \|u-v\|_{H^{-1}(S_L)}^2 & \text{if } (u, v) \in \mathcal{K}, \\ \infty & \text{otherwise,} \end{cases}$$

where the coefficients c_i are nonnegative (and not all equal to zero), S_L is a periodic strip $\mathbb{T}_L \times \mathbb{R}$ (where \mathbb{T}_L is the one-dimensional torus of length L), and the set of admissible functions is given by

$$\mathcal{K} := \left\{ (u, v) \in (\text{BV}(S_L))^2 : u(x), v(x) \in \{0, 1\} \text{ a.e., } uv = 0 \text{ a.e., and } \int_{S_L} u = \int_{S_L} v \right\}.$$

Since unconstrained minimisation will lead to the trivial structure $u \equiv v \equiv 0$, the natural problem to look at here is minimisation under constrained mass, i.e. with the constraint $\int_{S_L} u = \int_{S_L} v = M$ for some $M > 0$.

Under the extra restriction $u + v \equiv 1$ —no 0-phase—the functional \mathcal{F} is a well-known sharp-interface model for diblock copolymer melts [35, 9]. The sharp-interface character of this model, known in the physics literature as the strong-segregation limit, is recognizable in the fact that the variables u and v are characteristic functions, implying that at each point in space only one phase is present. The underlying diffuse-interface model is well studied [31, 16, 15, 30, 36, 9, 37, 40, 41, 42, 51, 43] because of the interesting pattern formation phenomena it exhibits.

The first three terms of \mathcal{F} can be recognised as the sharp-interface manifestation of the repelling forces between the U-, V-, and 0-monomers. The last term, the H^{-1} -norm, is a remainder of the chemical bond between the U- and V-parts and penalises large-scale separation of the U- and V-phases.

The functional \mathcal{F} resembles the energy functional used to model triblock copolymers, i.e. block copolymers consisting of three chemically bonded parts, [38, 39]. The interface penalisation part is present in that functional as well, and the long range interaction term includes interaction between the third phase (the phase corresponding to the third part of the triblock copolymers)

and the other two phases in addition to the interaction between the first two phases present in the functional \mathcal{F} above.

For a more extensive review of the modelling of diblock copolymers and diblock copolymer-homopolymer blends and its study in mathematics, we refer to [54, Chapter 2].

1.3 From one-dimensional to two-dimensional structures

A layered structure with perfectly straight layers can be described by functions u and v of one spatial variable. In a companion paper [17] (see also [8]) we study this one-dimensional case and give a full characterisation of global minimisers.

One of the results in that paper is that, for generic parameter values, every constrained-mass global minimiser on \mathbb{R} is a *concatenation of equal-width monolayers*. A monolayer is shown in Figure 1: a structure, described by a pair of functions (u, v) , in which the supports of u and v are adjacent intervals of equal length—or, in the higher-dimensional context, adjacent layers of equal width (see Figures 1a and 1c).

For small constrained mass, the global minimiser in one dimension is a monolayer. For slightly larger constrained mass, the global minimiser switches to a *bilayer*, a pair of monolayers joined back to back (Figures 1b and 1d). As the constrained mass further increases the global minimiser switches to structures of increasing numbers of monolayers (see [17]).

In the present paper we are interested in the stability properties under \mathcal{F} of a particular subset of two-dimensional mono- and bilayer structures:

- For both mono- and bilayers we assume that the layer thickness is such that the energy-to-mass ratio $\mathcal{F}/\int u$ is minimal among all such layers;
- For monolayers we assume that $c_u = c_v$, i.e. that the interface penalisation is the same for U-0 and V-0 interfaces.

Both restrictions arise from our interest in thin, partially localised structures in \mathbb{R}^2 , as is explained in detail in Appendices A and B.

The optimal widths δ_m and δ_b for which the energy-to-mass ratio is minimal for the mono- and bilayer respectively are indicated in Figure 1 and defined in (17) and (7).

1.4 Stability of mono- and bilayers in two dimensions

The aim of this paper is to investigate the stability of these mono- and bilayers in two dimensions. Since the functions u and v are forced to be characteristic functions of sets, the only admissible perturbations are changes in the supports of these functions. In this paper we only consider *local* stability with respect to perturbation of the position of the interfaces; other perturbations, such as those that change the topology of the structure are disregarded (see the discussion in Section 6).

Specifically, we consider perturbations of the interfaces that are periodic with period L along the length of the layer, and therefore we assume a domain that is periodic in one direction (x_1) and unbounded in the other (see Figure 1). Because of this periodicity each perturbation of an interface is given by a periodic function $p : \mathbb{T}_L \rightarrow \mathbb{R}^3$ (for the monolayer) or $p : \mathbb{T}_L \rightarrow \mathbb{R}^4$ (for the bilayer), where each component is the lateral displacement of one of the interfaces. By expanding the perturbations in Fourier modes, and using the usual vanishing of cross terms of different frequency, the positivity of the second derivative of the energy reduces to the positivity on each Fourier mode.¹

Fourier modes have a natural scale invariance: the k^{th} Fourier mode on the interval of length L is equivalent to the 1st Fourier mode on an interval of length L/k . This allows us to establish the stability with respect to the first Fourier mode as a function of L , rescale for the stability properties of the k^{th} mode, and aggregate the results.

¹First and second derivatives of similar functionals have been calculated by Muratov and Choksi & Sternberg [30, 10]. Our calculations differ in the number of phases (three instead of two) and in the early adoption of a Fourier framework.

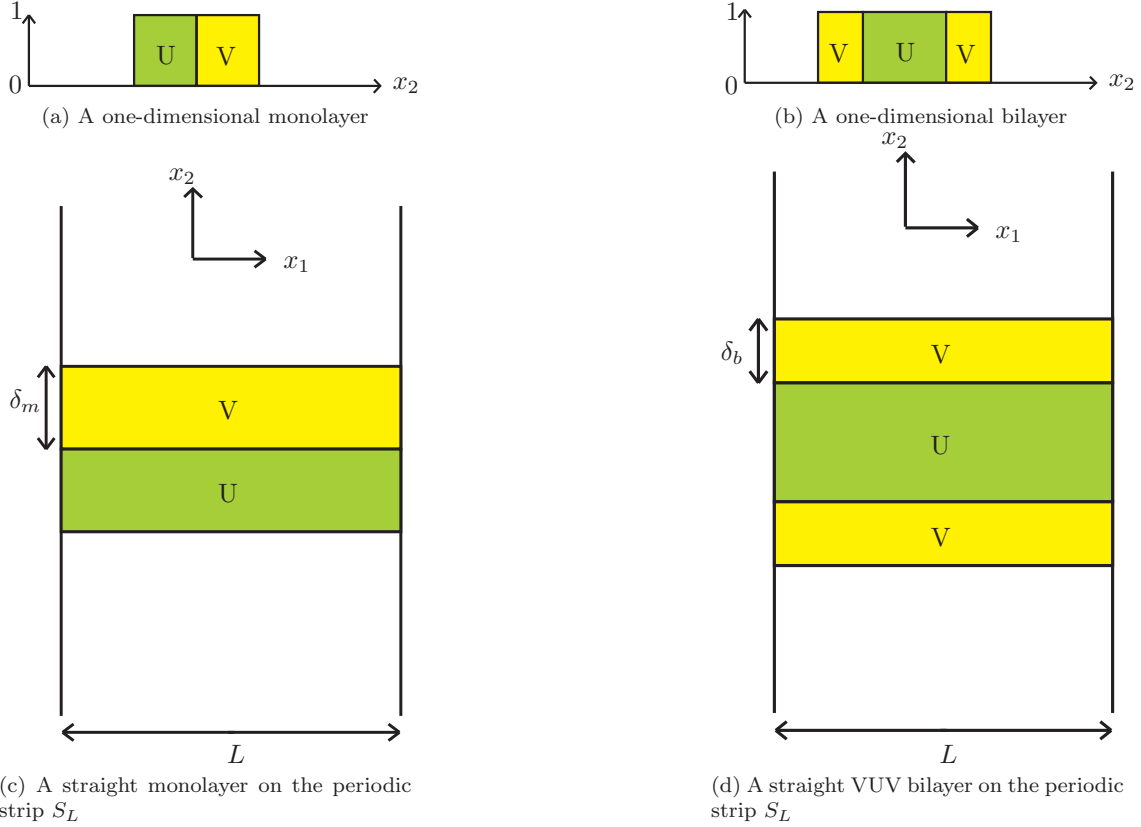


Figure 1: Mono- and bilayers on a strip as trivial extensions of one-dimensional structures. We assume the 0-phase to fill up the rest of the domain where there is no U- or V-phase. We do not indicate this in our pictures.

Using this approach we show in Section 4 that the monolayer of optimal width δ_m is linearly stable with respect to mode-1 perturbations iff

$$\frac{c_u}{2c_u + c_0} \geq f_1(L/\delta_m),$$

where f_1 is an explicit function given in (31). By combining all Fourier modes we find

Theorem 1.1. *Assume $c_u = c_v$. The monolayer of optimal width is linearly stable iff*

$$\frac{c_u}{2c_u + c_0} \geq f(L/\delta_m) \quad (1)$$

where

$$f(\ell) := \sup_{k \geq 1} f_1(\ell/k).$$

The graphs of the functions $x \mapsto f_1(x/k)$ for different values of k are shown in Figure 2a.

For a bilayer of optimal width δ_b a similar result holds:

Theorem 1.2. *The VUV bilayer of optimal width is linearly stable iff*

$$\frac{c_u + c_v}{c_0 + c_u + 2c_v} \geq g(L/\delta_b) \quad (2)$$

where

$$g(\ell) := \sup_{k \geq 1} g_1(\ell/k)$$

and g_1 is given by (24).

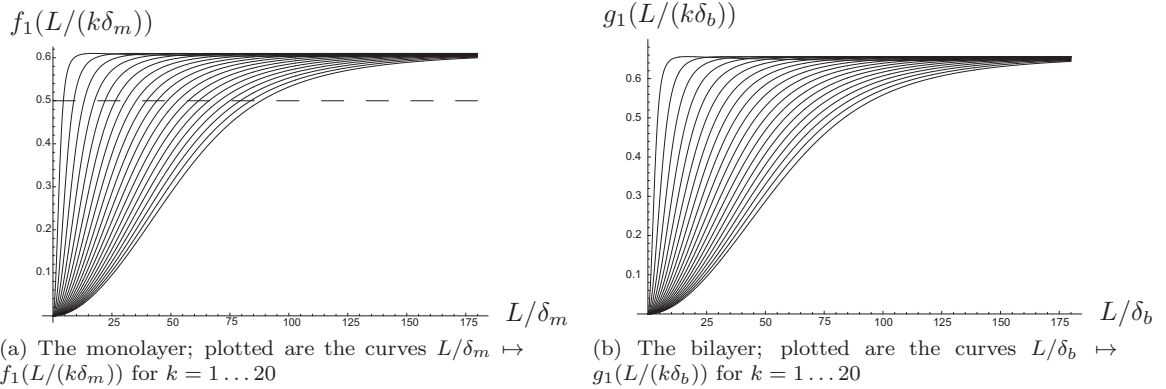


Figure 2: The graphs of the functions $x \mapsto f_1(x/k)$ and $x \mapsto g_1(x/k)$ ($k = 1, \dots, 20$) portray the curves in parameter space that separate the parts where the first twenty Fourier modes of the second variation for the monolayer (Figure 2a) and bilayer (Figure 2b) are positive and negative. If $c_u/(2c_u + c_0) < f_1(L/(k\delta_m))$ the k th Fourier mode is negative for the monolayer, if the reverse inequality holds the mode is positive. Similarly for the bilayer the k th Fourier mode is negative if $(c_u + c_v)/(c_0 + c_u + 2c_v) < g_1(L/(k\delta_b))$. The leftmost curve in each figure corresponds to the first order Fourier mode, the order increases towards the right. Note that the positivity of the parameters c_u and c_0 implies that $c_u/(2c_u + c_0) \leq \frac{1}{2}$ as indicated in Figure 2a by the dashed line.

In Figure 2b the graphs of the functions $x \mapsto g_1(x/k)$ are shown for different values of k .

From Figures 2a and 2b one might think that curves belonging to higher orders remain below curves of lower orders. The blow-ups in Figure 3 however show that this is not the case. However, it is true that only the first Fourier mode is of importance for determining the stability of the monolayer. This can be recognised by noting that the left-hand side of (1) cannot reach values larger than $1/2$, and Figures 2a and 3a show that the non-monotonicity for the monolayer plays a role only for values above $1/2$.

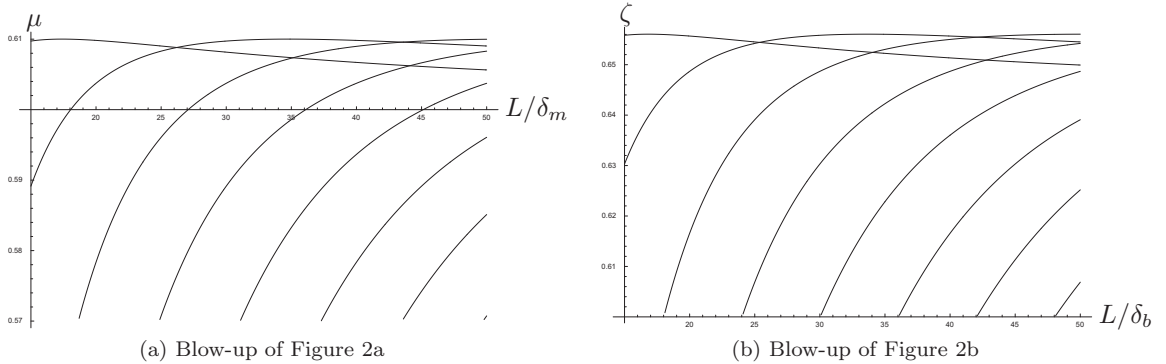


Figure 3: A blow-up of the graphs in Figure 2. Curves corresponding to different Fourier modes clearly cross. Here $\mu = \frac{c_u + c_v}{2(c_0 + c_u + c_v)}$ and $\zeta = \frac{c_u + c_v}{c_0 + c_u + 2c_v}$, see also (20) and (30).

Figure 4 summarises the stability properties of both the mono- and the bilayer. In Figure 4a the vertical axis is restricted to the interval $[0, 1/2]$ to reflect the value set of the left-hand side of (1). This implies that monolayers can only be stable if L is sufficiently small, and even then only for a subset of the coefficients c_0 , c_u , and c_v ; for sufficiently large L the monolayer is unstable for all choices of interface penalisation.

For the bilayer the situation is different: here the condition (2) allows for both stability and instability at all values of L . The function g is bounded from above (away from 1), implying that

a threshold α exists such that

$$\frac{c_u + c_v}{c_0 + c_u + 2c_v} \geq \alpha \quad \Longrightarrow \quad \text{Bilayer is stable for all } L.$$

From Figure 4b we estimate that $\alpha \approx 0.65$.

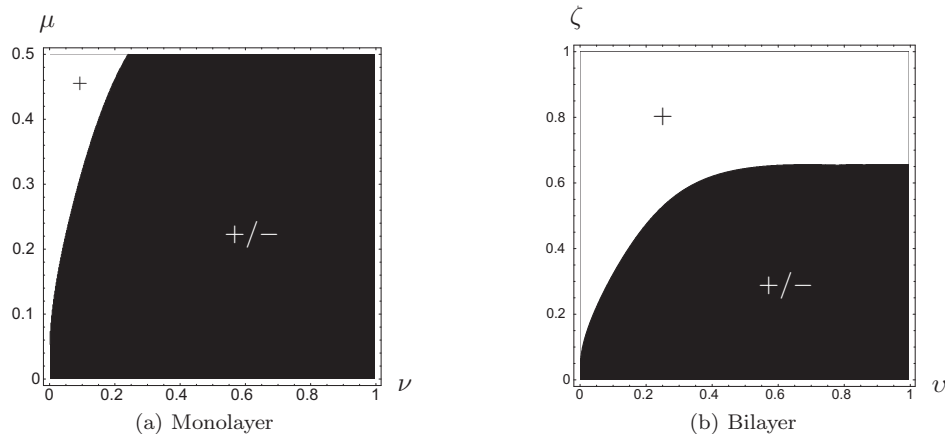


Figure 4: The sign of the second derivative operator for the mono- and bilayer of optimal width. $+/-$ indicates indeterminate sign, due to the negativity of one or more eigenvalues. Along the horizontal axes are plotted $\nu = e^{-2\pi\delta_m/L}$ and $\nu = e^{-2\pi\delta_b/L}$. The vertical axes show $\mu = c_u/(2c_u + c_0)$ and $\zeta = (c_u + c_v)/(c_0 + c_u + 2c_v)$. These figures are based on a calculation involving Fourier modes up to and including order 100.

1.5 Directions of instability

For the functional \mathcal{F} one may imagine a number of different evolution problems, such as gradient flows based on the L^2 , H^{-1} , or Wasserstein metrics. Under such an evolution the straight mono- and bilayer structures are stationary. If they are unstable, the evolution will amplify small deviations and move away from the straight configurations. While the perturbations are still small, the main contribution of the evolution will be in the directions of the eigenvectors of the second variation² belonging to the (most) negative eigenvalues.

For the monolayer there is, for each Fourier mode, one eigenvalue that can become negative (for the first Fourier mode: E_3 in Lemma 4.12; other modes follow by rescaling as above) and there are two which are always positive. Each component of the corresponding eigenvectors is associated with the deformation of one of the interfaces in the layer. A cartoon of the (possibly) unstable deformation direction is given in Figure 5a, the two stable directions are shown in Figures 5b and 5c.

For the bilayer two eigenvalues are always positive, and two eigenvalues may also become negative. For the first Fourier mode the dependence of the sign of the latter two on the parameters L/δ_b and ζ is given in Figures 6a and 6b. We recognise in the second figure the first order curve ($k = 1$) from Figure 2b; a similar curve for the first figure would always stay below the curve from the latter one, which is why its influence is not recognisable in Figure 2b.

The (possibly) unstable deformation directions are shown in Figures 7a and 7b, corresponding to the eigenvalues in Figures 6a and 6b, the stable ones in Figures 7c and 7d.

These results all show that depending on the parameters in the model the monolayer and bilayer structures can be unstable. This mirrors closely the results in [30], [37], and [40], where it is shown that in the pure diblock case ‘wriggled’ lamellar structures bifurcate off the straight

²For each Fourier mode the bilinear form that is the second variation can be identified with a bilinear form on \mathbb{R}^3 (monolayer) or \mathbb{R}^4 (bilayer) whose eigenvalues and eigenvectors can be studied. Details can be found in Sections 4.2–4.3.

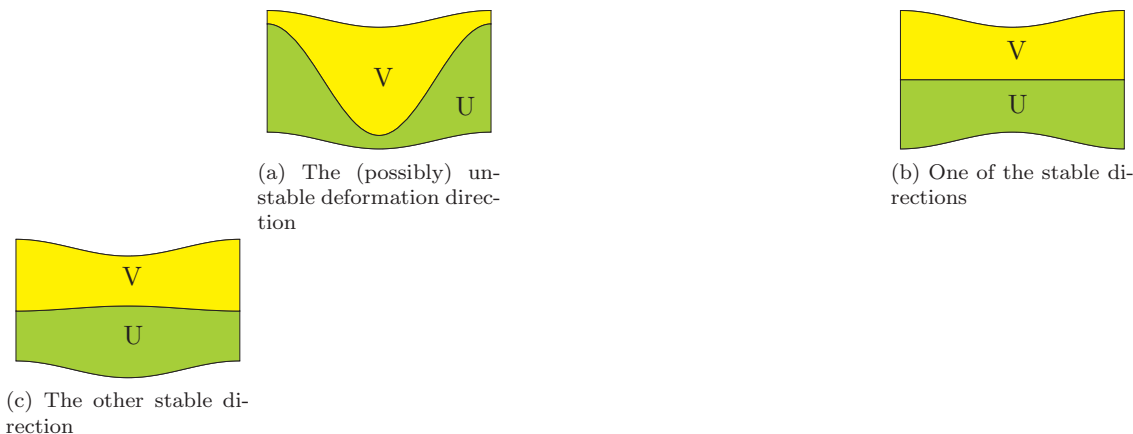


Figure 5: One (possibly) unstable and two stable first order Fourier modes of deformation for the monolayer; see Section 4, in particular Remark 4.17.

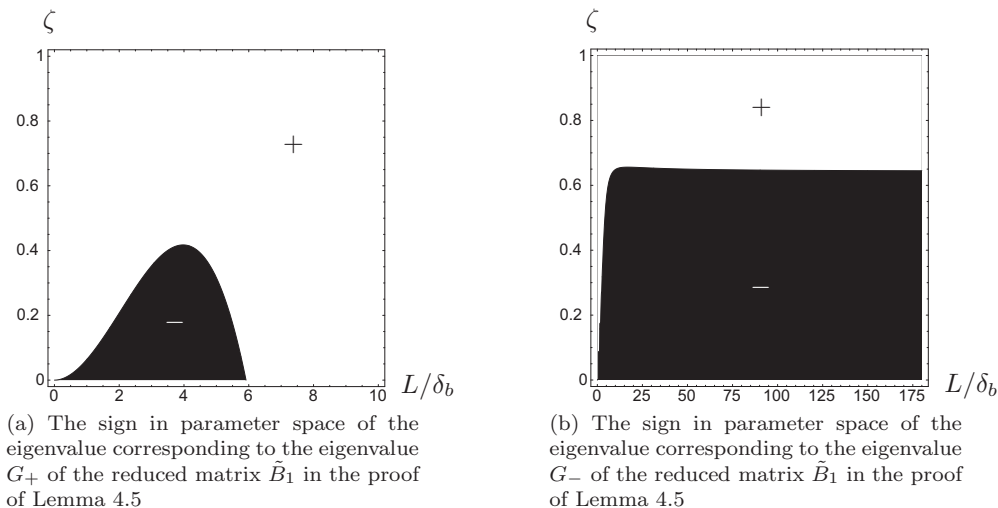


Figure 6: The black patches in parameter space indicate where two of the eigenvalues of the first Fourier order second variation operator for the bilayer become negative.

lamellar pattern if the spacing between the lamellae becomes too large. In Section 6.3 we discuss the relation with these results in more detail.

1.6 Structure of this paper

We start in Section 2 by defining the functional under consideration and clarifying some of the notation that is used throughout the paper. In Section 3 we prove via a calculation of the first variation of \mathcal{F} that the monolayer and bilayer are both stationary points of \mathcal{F} with respect to mass preserving perturbations of the interfaces. We then proceed to compute the second variation for both these structures. Since this calculation for the monolayer is similar to that for the bilayer, we only give the details in the latter case and even there we defer most of the computational details to Appendix C. Section 4 is dedicated to computing the sign of the second variations for the monolayer and bilayer in order to determine the parameter regions of stability and instability. Much of the work in the proofs is again of a calculational nature, some of which we have also moved to the back of the paper in Appendix D. Finally Section 5 gives a Green's function of $-\Delta$ on the periodic strip. This Green's function is heavily used in this paper and since the authors

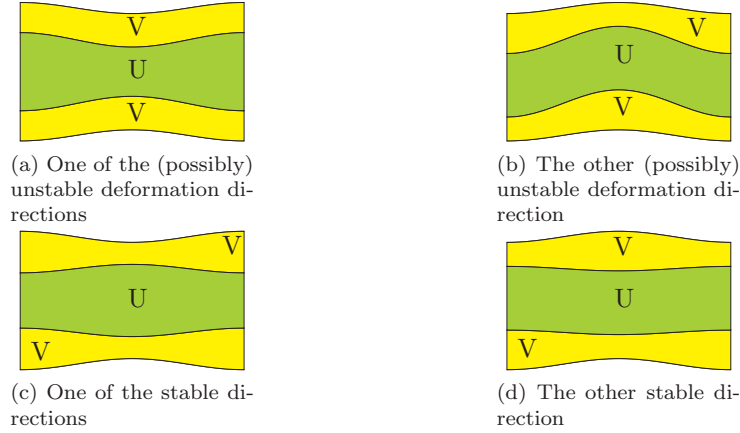


Figure 7: Two (possibly) unstable and two stable first-order Fourier modes of deformation for the bilayer. The (possibly) unstable deformation in Figure 7a corresponds to the eigenvalue in Figure 6a and the deformation in Figure 7b to the eigenvalue in Figure 6b. For details see the discussion in Section 4, in particular Remark 4.10.

could not trace a previous appearance of it in the literature a section on its validity closes this paper.

2 Definitions and conventions

2.1 Problem setting

The domain of definition is the strip $S_L := \mathbb{T}_L \times \mathbb{R}$, where \mathbb{T}_L is the one-dimensional torus of length L , i.e. the interval $[0, L]$ with the endpoints identified. For functions on S_L the H^{-1} -norm is defined by convolution:

Definition 2.1. For $f \in L^\infty(S_L)$ with compact support satisfying $\int_{S_L} f = 0$ we define

$$\|f\|_{H^{-1}(S_L)}^2 := \int_0^L \int_{\mathbb{R}} f(x_1, x_2) G * f(x_1, x_2) dx_2 dx_1,$$

where G is the Green's function of the operator $-\Delta$ on S_L , i.e. it satisfies $-\Delta G = \delta$ in the sense of distributions (δ is the Dirac delta distribution).

Note that $\phi_f := G * f$ satisfies $-\Delta \phi_f = f$ on S_L . Also note that while the Green's function is only unique up to addition of an affine function of x_2 , this non-uniqueness is irrelevant for the definition above.

We repeat the definition of \mathcal{F} and \mathcal{K} for convenience.

Definition 2.2. Let c_0 , c_u , and c_v be real numbers. Define

$$\mathcal{F}(u, v) = \begin{cases} c_0 \int_{S_L} |\nabla(u+v)| + c_u \int_{S_L} |\nabla u| + c_v \int_{S_L} |\nabla v| + \|u-v\|_{H^{-1}(S_L)}^2 & \text{if } (u, v) \in \mathcal{K}, \\ \infty & \text{otherwise,} \end{cases}$$

where the admissible set is given by

$$\mathcal{K} := \left\{ (u, v) \in (BV(S_L))^2 : u(x), v(x) \in \{0, 1\}, uv = 0 \text{ a.e., and } \int_{S_L} u = \int_{S_L} v \right\}.$$

We will require that all c_i are non-negative and at least one of them is positive.

Another, equivalent, form of the functional will be useful, in which the penalisation of the three types of interface U-0, V-0, and U-V, is given explicitly by surface tension coefficients d_{kl} :

Lemma 2.3. *Let the surface tension coefficients be given by*

$$\begin{aligned} d_{u0} &:= c_u + c_0, \\ d_{v0} &:= c_v + c_0, \\ d_{uv} &:= c_u + c_v. \end{aligned}$$

*Non-negativity of the c_i is equivalent to the conditions*³

$$0 \leq d_{kl} \leq d_{kj} + d_{jl} \quad \text{for each } k \neq l \neq j \neq k. \quad (3)$$

Then

$$\mathcal{F}(u, v) = \begin{cases} d_{u0} \mathcal{H}^{N-1}(S_{u0}) + d_{v0} \mathcal{H}^{N-1}(S_{v0}) + d_{uv} \mathcal{H}^{N-1}(S_{uv}) + \|u - v\|_{H^{-1}(S_L)}^2 & \text{if } (u, v) \in \mathcal{K}, \\ \infty & \text{otherwise.} \end{cases}$$

where S_{kl} is the interface between the phases k and l :

$$\begin{aligned} S_{u0} &= \partial^* \text{supp } u \setminus \partial^* \text{supp } v, \\ S_{v0} &= \partial^* \text{supp } v \setminus \partial^* \text{supp } u, \\ S_{uv} &= \partial^* \text{supp } u \cap \partial^* \text{supp } v, \end{aligned}$$

and ∂^* is the essential boundary of a set.

The essential boundary of a set consists of all points in the set that have a density other than 0 or 1 in the set; see e.g. [4, Chapter 3.5].

Proof of Lemma 2.3. The main step in recognising the equivalence of both forms of \mathcal{F} is noticing that, for characteristic functions of a set, such as u, v and $u + v$, the equality

$$\int_{\Omega} |\nabla u| = \mathcal{H}^{N-1}(\partial^* \text{supp } u \cap \Omega)$$

(see [18, Theorem 4.4], [4, Theorems 3.59, 3.61]). □

Note the different interpretations of the coefficients c_i and the surface tension coefficients d_{kl} . The latter have a direct physical interpretation (and can be related to material parameters, see [8]): they determine the mutual repulsion between the different constituents of the diblock copolymer-homopolymer blend. For example, the value of d_{uv} (as compared to the values of d_{u0} , d_{v0} and 1, the coefficient in front of the H^{-1} -norm) determines the energy penalty associated with close proximity of U- and V-polymers. In particular, if one of these surface tension coefficients is zero, the corresponding polymers do not repel each other and many interfaces between their respective phases in the model can be expected. On the other hand the coefficients c_i , when taken separately, do not convey complete information about the penalisation of the boundary of a phase. If for instance $c_u = 0$, but $c_v \neq 0$, the part of the U-phase interface that borders on the V-phase still receives a penalty, because $d_{uv} = c_v$. For this reason the use of surface tension coefficients makes more sense from a physical point of view. For the mathematics it is often easier to use the formulation in terms of c_i .

If we consider the functional \mathcal{F} on three-dimensional ‘physical space’ we can also see from dimensional considerations that the name “surface tension coefficients” for the d_{kl} is justified. Since $\mathcal{H}^2(S_{kl})$ measures surface area, if \mathcal{F} has the dimension of energy then the coefficients d_{kl} have the dimension of energy per unit area, which is also the dimension of surface tension.

³The indices j, k, l take values in $\{u, v, 0\}$ and the d_{kl} are taken symmetric in their indices, i.e. $d_{vu} = d_{uv}$ etc.

Remark 2.4. The conditions (3) can be understood in several ways. If, for instance, $d_{uv} > d_{u0} + d_{v0}$, then the U-V type interface, which is penalised with a weight of d_{uv} , is unstable, for the energy can be reduced by slightly separating the U and V regions and creating a thin zone of 0 inbetween. A different way of seeing the necessity of (3) is by remarking that the equivalent requirement of non-negativity of the c_i is necessary for \mathcal{F} to be lower semicontinuous in e.g. the L^1 topology (see e.g. [18, Theorem 1.9]). Our assumption that at least one c_i is positive is equivalent to requiring at least two d_{kl} to be positive.

2.2 Fourier transformation

To clarify the notation we use, we will explicitly define the Fourier series we are using. For future reference we will also state some results we will need.

Definition 2.5. Let $f \in L^2(\mathbb{T}_L)$, then we will denote by $\hat{f} \in L^2(\mathbb{Z}; \mathbb{C})$, the Fourier transform of f :

$$\hat{f}(k) := \frac{1}{\sqrt{L}} \int_0^L f(x) e^{-2\pi i x k / L} dx,$$

and by a_j and b_j , $j \in \mathbb{N}$, the Fourier coefficients of f with respect to the normalised basis of cosines and sines:

$$\begin{aligned} a_0 &:= \frac{1}{\sqrt{L}} \int_0^L f(x) dx, \\ a_j &:= \sqrt{\frac{2}{L}} \int_0^L f(x) \cos\left(\frac{2\pi x j}{L}\right) dx, \\ b_j &:= \sqrt{\frac{2}{L}} \int_0^L f(x) \sin\left(\frac{2\pi x j}{L}\right) dx, \end{aligned}$$

For easy reference we give here the relations between $\hat{f}(j)$ and a_j, b_j : $\hat{f}(0) = a_0$ and, for $j \geq 1$, $\hat{f}(j) = \frac{1}{\sqrt{2}}(a_j - ib_j)$, $\hat{f}(-j) = \frac{1}{\sqrt{2}}(a_j + ib_j)$, $a_j = \frac{1}{\sqrt{2}}(\hat{f}(j) + \hat{f}(-j))$ and $b_j = \frac{i}{\sqrt{2}}(\hat{f}(j) - \hat{f}(-j))$.

Furthermore we have

$$\begin{aligned} f(x) &= \frac{a_0}{\sqrt{L}} + \sqrt{\frac{2}{L}} \sum_{j=1}^{\infty} a_j \cos(2\pi x j / L) + \sqrt{\frac{2}{L}} \sum_{j=1}^{\infty} b_j \sin(2\pi x j / L), \\ f(x) &= \frac{1}{\sqrt{L}} \sum_{q \in \mathbb{Z}} \hat{f}(q) e^{2\pi i x q / L}, \end{aligned}$$

where the convergence is in the L^2 topology. Finally Parseval's theorem takes the form

$$\begin{aligned} \int_0^L f(x) g(x) dx &= \hat{f}(0) \hat{g}(0) + 2\operatorname{Re} \sum_{q=1}^{\infty} \hat{f}(q) \overline{\hat{g}(q)} \\ &= a_{f,0} a_{g,0} + \sum_{j=1}^{\infty} [a_{f,j} a_{g,j} + b_{f,j} b_{g,j}], \end{aligned} \quad (4)$$

and as a consequence we have for $p_1, p_2, p_3 \in L^2(\mathbb{T}_L)$

$$\int_{\mathbb{T}_L} \int_{\mathbb{T}_L} p_1(x) p_2(x-y) p_3(y) dx dy = L^{1/2} \sum_{q \in \mathbb{Z}} \hat{p}_1(q) \overline{\hat{p}_2(q)} \hat{p}_3(q). \quad (5)$$

3 Geometrical derivatives of the energy

In the following two sections we will take a look at the stability of two-dimensional periodic monolayer and bilayer configurations. First we need to determine under which conditions these structures are stationary points of the functional \mathcal{F} . For the bilayer this will be done in Section 3.1, after which we compute the second variation for a bilayer in Section 3.2. We will give analogous results for the monolayer in Section 3.3. In Section 4 we will use these results to derive the explicit stability criteria of Theorems 1.1 and 1.2.

Of the two possible bilayer structures—UVU and VUV—we only discuss the VUV structure. The results for the UVU structure follow from exchanging the roles of u and v .

3.1 Bilayer: admissible perturbations and stationarity

The VUV bilayer of optimal width is a structure given by functions $(u_0, v_0) \in \mathcal{K}$ with

$$u_0 := \chi_{\mathbb{T}_L \times [-\delta_b, \delta_b]} \quad \text{and} \quad v_0 := \chi_{\mathbb{T}_L \times ([-2\delta_b, -\delta_b] \cup [\delta_b, 2\delta_b])}, \quad (6)$$

where [17]

$$\delta_b := \sqrt[3]{\frac{3}{4}(c_0 + c_u + 2c_v)}, \quad (7)$$

and χ_A is the characteristic function of the set A . The set of admissible boundary perturbations of this structure is only restricted by regularity and the equal-mass constraint:

Definition 3.1. *The set of admissible perturbations is characterised by*

$$\mathcal{P}_b := \left\{ p \in (W^{1,2}(\mathbb{T}_L))^4 : 2 \int_{\mathbb{T}_L} (p_1 + p_3) = \int_{\mathbb{T}_L} (p_2 + p_4) \right\}. \quad (8)$$

For $p \in \mathcal{P}_b$ and $\varepsilon > 0$ we define a perturbed structure $(u_\varepsilon, v_\varepsilon)$,

$$u_\varepsilon(x_1, x_2) = \begin{cases} 1 & \text{if } x_2 \in (-\delta_b - \varepsilon p_3(x_1), \delta_b + \varepsilon p_1(x_1)), \\ 0 & \text{otherwise,} \end{cases}$$

$$v_\varepsilon(x_1, x_2) = \begin{cases} 1 & \text{if } x_2 \in (-2\delta_b - \varepsilon p_4(x_1), -\delta_b - \varepsilon p_3(x_1)) \cup (\delta_b + \varepsilon p_1(x_1), 2\delta_b + \varepsilon p_2(x_1)), \\ 0 & \text{otherwise.} \end{cases}$$

We also introduce the subset of perturbations that conserve mass:

$$\mathcal{P}_b^M := \left\{ p \in \mathcal{P}_b : \int_{\mathbb{T}_L} (p_1 + p_3) = \int_{\mathbb{T}_L} (p_2 + p_4) = 0 \right\} \quad (9)$$

Note that since $W^{1,2}(\mathbb{T}_L)$ is imbedded in $L^\infty(\mathbb{T}_L)$ by the Sobolev imbedding theorem, the pair $(u_\varepsilon, v_\varepsilon)$ belongs to \mathcal{K} for sufficiently small ε .

A picture of a bilayer of optimal width with perturbations p is shown in Figure 8.

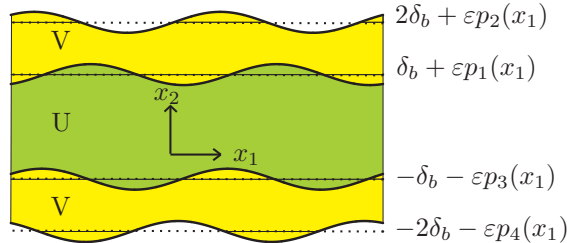


Figure 8: The bilayer of optimal width with perturbations

Remark 3.2. We should stress the difference between the two mass constraints (8) and (9). The constraint (8) is equivalent to the condition that u_ε and v_ε have the same mass. This property is a basic element of the model of block copolymers, via the set of admissible functions \mathcal{K} .

The additional condition (9) expresses the requirement that $\int u_\varepsilon$ and $\int v_\varepsilon$ both equal the mass $\int u_0$ of the unperturbed bilayer; perturbations without this property are meaningful in a situation where the joint mass of u_ε and v_ε may change. The bilayer of optimal width is a stationary point of the functional \mathcal{F} under mass-preserving changes (see Lemma 3.4 below); but as can be inferred from equation (13), the functional is *not* stationary under perturbations that do change the mass.

Definition 3.3. We say that the bilayer of optimal width is stationary with respect to the admissible perturbations \mathcal{P}_b (or \mathcal{P}_b^M) if, for all $p \in \mathcal{P}_b$ (or all $p \in \mathcal{P}_b^M$),

$$\left. \frac{d}{d\varepsilon} \mathcal{F}(u_\varepsilon, v_\varepsilon) \right|_{\varepsilon=0} = 0.$$

Lemma 3.4. The VUV bilayer of optimal width is stationary with respect to all $p \in \mathcal{P}_b^M$.

Proof. Choksi and Sternberg calculate the first and second variations of a related functional [10], and their method can be adapted without much difficulty to the functional \mathcal{F} . Here we give a self-contained proof.

Since the interfaces of the bilayer are straight, the derivative of the interfacial terms with respect to the perturbation is zero for all $p \in \mathcal{P}_b$:

$$\begin{aligned} & \left. \frac{d}{d\varepsilon} \left(c_0 \int_{S_L} |\nabla(u_\varepsilon + v_\varepsilon)| + c_u \int_{S_L} |\nabla u_\varepsilon| + c_v \int_{S_L} |\nabla v_\varepsilon| \right) \right|_{\varepsilon=0} \\ &= \left. \frac{d}{d\varepsilon} \left[d_{uv} \int_0^L \left(\sqrt{1 + \varepsilon^2 p_1'^2} + \sqrt{1 + \varepsilon^2 p_3'^2} \right) dx + d_{v0} \int_0^L \left(\sqrt{1 + \varepsilon^2 p_2'^2} + \sqrt{1 + \varepsilon^2 p_4'^2} \right) dx \right] \right|_{\varepsilon=0} \\ &= 0. \end{aligned} \tag{10}$$

For the derivative of the H^{-1} -norm, let $\eta \in C(\mathbb{R})$ and compute

$$\begin{aligned} \left. \frac{d}{d\varepsilon} \int_{S_L} \eta(x_2) u_\varepsilon(x) dx \right|_{\varepsilon=0} &= \int_0^L \left. \frac{d}{d\varepsilon} \int_{-\delta_b - \varepsilon p_3(x_1)}^{\delta_b + \varepsilon p_1(x_1)} \eta(x_2) dx_2 \right|_{\varepsilon=0} dx_1 \\ &= \int_0^L \left(p_1(x_1) \eta(\delta_b + \varepsilon p_1(x_1)) + p_3(x_1) \eta(-\delta_b - \varepsilon p_3(x_1)) \right) dx_1 \Big|_{\varepsilon=0} \\ &= \eta(\delta_b) \int_0^L p_1 + \eta(-\delta_b) \int_0^L p_3. \end{aligned} \tag{11}$$

Similarly,

$$\left. \frac{d}{d\varepsilon} \int_{S_L} \eta(x_2) v_\varepsilon(x) dx \right|_{\varepsilon=0} = -\eta(\delta_b) \int_0^L p_1 + \eta(2\delta_b) \int_0^L p_2 - \eta(-\delta_b) \int_0^L p_3 + \eta(-2\delta_b) \int_0^L p_4. \tag{12}$$

Let G be the Green's function of $-\Delta$ on S_L from Theorem 5.1, then

$$\begin{aligned} \left. \frac{d}{d\varepsilon} \|u_\varepsilon - v_\varepsilon\|_{H^{-1}(S_L)}^2 \right|_{\varepsilon=0} &= \left. \frac{d}{d\varepsilon} \int_{S_L} |\nabla G * (u_\varepsilon - v_\varepsilon)|^2 dx \right|_{\varepsilon=0} \\ &= 2 \int_{S_L} \nabla G * (u_0 - v_0) \left[\left. \frac{d}{d\varepsilon} \nabla G * (u_\varepsilon - v_\varepsilon) \right]_{\varepsilon=0} dx \\ &= 2 \left. \frac{d}{d\varepsilon} \int_{S_L} \nabla G * (u_0 - v_0) \cdot \nabla G * (u_\varepsilon - v_\varepsilon) dx \right|_{\varepsilon=0} \\ &= 2 \left. \frac{d}{d\varepsilon} \int_{S_L} [G * (u_0 - v_0)] (u_\varepsilon - v_\varepsilon) dx \right|_{\varepsilon=0} \end{aligned}$$

Setting $\eta(x_2) := [G^*(u_0 - v_0)](x_1, x_2)$ (which is independent of x_1 , because $u_0 - v_0$ is independent of x_1) we calculate by the Fourier series (33) (or by remarking that this is a one-dimensional situation) that

$$\eta(x_2) = -\frac{1}{2} \int_{\mathbb{R}} |x_2 - y| (u_0 - v_0)(0, y) dy,$$

from which it follows that $\eta(\delta_b) = \eta(-\delta_b)$ and $\eta(\pm 2\delta_b) = 0$. Therefore $\eta \in C(\mathbb{R})$ and thus we obtain from (11) and (12) that

$$\left. \frac{d}{d\varepsilon} \|u_\varepsilon - v_\varepsilon\|_{H^{-1}(S_L)}^2 \right|_{\varepsilon=0} = 4L\eta(\delta_b) \int (p_1 + p_3) \stackrel{(9)}{=} 0. \quad (13)$$

□

Remark 3.5. Note that in Lemma 3.4 we nowhere use the specific definition of δ_b in (7). As we explain in Appendix A the optimal width is relevant when considering energy per unit mass. If we define the mass functional as

$$\mathcal{M}(u, v) := \int_{S_L} u$$

for $(u, v) \in \mathcal{K}$, then the following calculations show that the bilayer of optimal width is a stationary point of \mathcal{F}/\mathcal{M} with respect to all perturbations in \mathcal{P}_b (so not only the mass preserving ones) in the sense of Definition 3.3 (with the functional \mathcal{F} replaced by \mathcal{F}/\mathcal{M}). Thus, let now $p \in \mathcal{P}_b$.

We first compute that $\eta(\delta_b) = \frac{1}{2}\delta_b^2$, where η is such as chosen at the end of the proof of Lemma 3.4. Then with the help of (13) and the computations for the one-dimensional case in [17] we find that

$$\begin{aligned} \left. \frac{d}{d\varepsilon} \mathcal{F}(u_\varepsilon, v_\varepsilon) \right|_{\varepsilon=0} &= 2\delta_b^2 \int_0^L (p_1 + p_3), \\ \left. \frac{d}{d\varepsilon} \mathcal{M}(u_\varepsilon, v_\varepsilon) \right|_{\varepsilon=0} &= \int_0^L (p_1 + p_3), \\ \mathcal{F}(u_0, v_0) &= 2L(c_0 + c_u + 2c_v) + \frac{4}{3}L\delta_b^3, \\ \mathcal{M}(u_0, v_0) &= 2L\delta_b. \end{aligned}$$

Now we conclude

$$\begin{aligned} \left. \frac{d}{d\varepsilon} \mathcal{F}/\mathcal{M}(u_\varepsilon, v_\varepsilon) \right|_{\varepsilon=0} &= \mathcal{M}(u_0, v_0)^{-2} \left(\mathcal{M}(u_0, v_0) \left. \frac{d}{d\varepsilon} \mathcal{F}(u_\varepsilon, v_\varepsilon) \right|_{\varepsilon=0} + \right. \\ &\quad \left. - \mathcal{F}(u_0, v_0) \left. \frac{d}{d\varepsilon} \mathcal{M}(u_\varepsilon, v_\varepsilon) \right|_{\varepsilon=0} \right) \\ &= \frac{1}{2}L^{-1}\delta_b^{-2} \int_0^L (p_1 + p_3) \left(\frac{4}{3}\delta_b^3 - (c_0 + c_u + 2c_v) \right) \\ &\stackrel{(7)}{=} 0. \end{aligned}$$

We see that the optimal width condition (7) is not necessary for stationarity under \mathcal{F}/\mathcal{M} with respect to the mass preserving perturbations in \mathcal{P}_b^M , but it is for stationarity with respect to perturbations in $\mathcal{P}_b \setminus \mathcal{P}_b^M$.

3.2 Second variation for a bilayer

We express the components p_i of a given perturbation $p \in \mathcal{P}_b$ as a Fourier series (see Section 2.2):

$$p_i(x) = \frac{a_{i,0}}{\sqrt{L}} + \sqrt{\frac{2}{L}} \sum_{j=1}^{\infty} a_{i,j} \cos\left(\frac{2\pi x j}{L}\right) + \sqrt{\frac{2}{L}} \sum_{j=1}^{\infty} b_{i,j} \sin\left(\frac{2\pi x j}{L}\right). \quad (14)$$

The equal-mass condition in (8) translates into

$$2(a_{1,0} + a_{3,0}) = a_{2,0} + a_{4,0}. \quad (15)$$

We also write

$$\mathbf{a}_j := (a_{1,j}, a_{2,j}, a_{3,j}, a_{4,j}) \quad \text{and} \quad \mathbf{b}_j := (b_{1,j}, b_{2,j}, b_{3,j}, b_{4,j}).$$

Theorem 3.6. *Using the notation introduced above, the second variation of \mathcal{F} at the VUV bilayer of optimal width (6) in the direction $p \in \mathcal{P}_b$ is given by*

$$\left. \frac{d^2}{d\varepsilon^2} \mathcal{F}(u_\varepsilon, v_\varepsilon) \right|_{\varepsilon=0} = B_0(\mathbf{a}_0, \delta_b) + \sum_{j=1}^{\infty} B_j(\mathbf{a}_j, \mathbf{b}_j, d_{uv}, d_{v0}, L),$$

where

$$B_0(\mathbf{a}_0, \delta_b) := 4\delta_b \left\{ -a_{1,0}^2 - a_{3,0}^2 + a_{1,0}a_{2,0} + a_{3,0}a_{4,0} - 4a_{1,0}a_{3,0} + 3a_{2,0}a_{3,0} + 3a_{1,0}a_{4,0} - 2a_{2,0}a_{4,0} \right\},$$

and, for $j \in \mathbb{N}_{>0}$,

$$\begin{aligned} B_j(\mathbf{a}_j, \mathbf{b}_j, d_{uv}, d_{v0}, L) := & \frac{4\pi^2 j^2}{L^2} [d_{uv} \{a_{1,j}^2 + a_{3,j}^2 + b_{1,j}^2 + b_{3,j}^2\} + d_{v0} \{a_{2,j}^2 + a_{4,j}^2 + b_{2,j}^2 + b_{4,j}^2\}] \\ & + \frac{L}{\pi j} \left[2 \left(1 - \frac{2\pi\delta_b j}{L} \right) \{a_{1,j}^2 + a_{3,j}^2 + b_{1,j}^2 + b_{3,j}^2\} \right. \\ & \quad + \frac{1}{2} \{a_{2,j}^2 + a_{4,j}^2 + b_{2,j}^2 + b_{4,j}^2\} \\ & \quad - 2 \{a_{1,j}a_{2,j} + a_{3,j}a_{4,j} + b_{1,j}b_{2,j} + b_{3,j}b_{4,j}\} e^{-2\pi\delta_b j/L} \\ & \quad + 4 \{a_{1,j}a_{3,j} + b_{1,j}b_{3,j}\} e^{-4\pi\delta_b j/L} \\ & \quad - 2 \{a_{1,j}a_{4,j} + a_{2,j}a_{3,j} + b_{1,j}b_{4,j} + b_{2,j}b_{3,j}\} e^{-6\pi\delta_b j/L} \\ & \quad \left. + \{a_{2,j}a_{4,j} + b_{2,j}b_{4,j}\} e^{-8\pi\delta_b j/L} \right]. \end{aligned}$$

The proof is given in Appendix C.

3.3 Variations for a monolayer

Analogous results also hold for monolayers as defined below. In the current subsection we will state them. Since the proofs are completely analogous to the proofs for bilayers, we will not write them out here.

The monolayer of optimal width is a structure given by functions $(u_0, v_0) \in \mathcal{K}$ with

$$u_0 := \chi_{\mathbb{T}_L \times [0, \delta_m]} \quad \text{and} \quad v_0 := \chi_{\mathbb{T}_L \times [\delta_m, 2\delta_m]}, \quad (16)$$

where [17]

$$\delta_m := \sqrt[3]{\frac{3}{2}(c_0 + c_u + c_v)}. \quad (17)$$

The set of admissible boundary perturbations of this structure is again restricted by regularity and the equal-mass constraint:

Definition 3.7. *The set of admissible perturbations is characterised by*

$$\mathcal{P}_m := \left\{ p \in (W^{1,2}(\mathbb{T}_L))^3 : \int_{\mathbb{T}_L} (p_2 - p_1) = \int_{\mathbb{T}_L} (p_3 - p_2) \right\}.$$

For $p \in \mathcal{P}_m$ and $\varepsilon > 0$ we define a perturbed structure $(u_\varepsilon, v_\varepsilon)$,

$$u_\varepsilon(x_1, x_2) = \begin{cases} 1 & \text{if } x_2 \in (\varepsilon p_1(x_1), \delta_m + \varepsilon p_2(x_1)), \\ 0 & \text{otherwise,} \end{cases}$$

$$v_\varepsilon(x_1, x_2) = \begin{cases} 1 & \text{if } x_2 \in (\delta_m + \varepsilon p_2(x_1), 2\delta_m + \varepsilon p_3(x_1)), \\ 0 & \text{otherwise.} \end{cases}$$

We also define the subset of mass preserving perturbations:

$$\mathcal{P}_m^M := \left\{ p \in \mathcal{P}_m : \int_{\mathbb{T}_L} (p_2 - p_1) = \int_{\mathbb{T}_L} (p_3 - p_2) = 0 \right\}. \quad (18)$$

A picture of a monolayer of optimal width with perturbations p is shown in Figure 9.

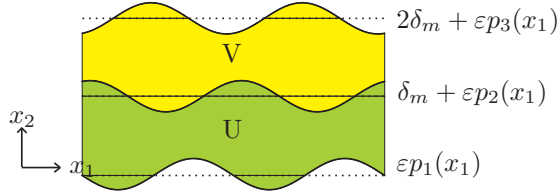


Figure 9: The monolayer of optimal width with perturbations

Stationarity for the monolayer of optimal width is defined analogously to stationarity for the bilayer, see Definition 3.3.

Lemma 3.8. *The monolayer of optimal width is stationary with respect to all $p \in \mathcal{P}_m^M$.*

Proof. Analogous to the proof of Lemma 3.4 we find that the first variation of the interfaces with respect to all $p \in \mathcal{P}_m$ is zero.

For any $\eta \in C(\mathbb{R})$ we compute

$$\frac{d}{d\varepsilon} \int_{S_L} \eta(x_2) u_\varepsilon(x) dx \Big|_{\varepsilon=0} = \eta(\delta_m) \int_0^L p_2 - \eta(0) \int_0^L p_1,$$

$$\frac{d}{d\varepsilon} \int_{S_L} \eta(x_2) v_\varepsilon(x) dx \Big|_{\varepsilon=0} = \eta(2\delta_m) \int_0^L p_3 - \eta(\delta_m) \int_0^L p_2.$$

With G the Green's function of $-\Delta$ on S_L from Theorem 5.1 we make the choice $\eta(x_2) = G * (u_0 - v_0)(x_1, x_2)$, which is independent of x_1 . Using $\eta(\delta_m) = 0$ and $\eta(0) = -\eta(2\delta_m) > 0$, we compute, as in the above mentioned proof,

$$\frac{d}{d\varepsilon} \|u_\varepsilon - v_\varepsilon\|_{H^{-1}(S_L)}^2 = 2\eta(0) \int_0^L (p_3 - p_1) \stackrel{(18)}{=} 0. \quad (19)$$

□

Note that by equation (19) the monolayer of optimal width is not stable with respect to perturbations that are allowed to change the total mass, i.e with respect to $p \in \mathcal{P}_m \setminus \mathcal{P}_m^M$.

Remark 3.9. In complete analogy to Remark 3.5 we see that the optimal width condition (17) plays no role in the stationarity of the monolayer under the functional \mathcal{F} , but it plays an important role when considering the stationarity of the monolayer under \mathcal{F}/\mathcal{M} , the energy per unit mass functional. Appendix A also argues the relevance of optimal width when considering energy per unit mass. Using, [17],

$$\mathcal{F}(u_0, v_0) = 2L(c_0 + c_u + c_v) + \frac{2}{3}L\delta_m^3,$$

a computation analogous to that in Remark 3.5 shows that the optimal width condition (17) is not necessary for stationarity under \mathcal{F}/\mathcal{M} with respect to the mass preserving perturbations in \mathcal{P}_m^M , but it is for stationarity with respect to perturbations in $\mathcal{P}_m \setminus \mathcal{P}_m^M$.

Similar to (14) we express a $p \in \mathcal{P}_m$ in terms of its Fourier modes $a_{i,j}$ and $b_{i,j}$ and introduce the notation

$$\mathbf{a}_j := (a_{1,j}, a_{2,j}, a_{3,j}) \quad \text{and} \quad \mathbf{b}_j := (b_{1,j}, b_{2,j}, b_{3,j}).$$

Theorem 3.10. *Using the notation given above, the second variation of \mathcal{F} at (u_0, v_0) in the direction of $p \in \mathcal{P}_m$ is given by*

$$\left. \frac{d^2}{d\varepsilon^2} \mathcal{F}(u_\varepsilon, v_\varepsilon) \right|_{\varepsilon=0} = M_0(\mathbf{a}_0, \delta_m) + \sum_{j=1}^{\infty} M_j(\mathbf{a}_j, \mathbf{b}_j, d_{u0}, d_{uv}, d_{v0}, L),$$

where

$$M_0(\mathbf{a}_0, \delta_m) := \delta_m (a_{1,0} - a_{3,0})^2,$$

and, for $j \in \mathbb{N}$,

$$\begin{aligned} M_j(\mathbf{a}_j, \mathbf{b}_j, d_{u0}, d_{uv}, d_{v0}, L) := & \\ & \frac{4\pi^2 j^2}{L^2} [d_{u0} \{a_{1,j}^2 + b_{1,j}^2\} + d_{uv} \{a_{2,j}^2 + b_{2,j}^2\} + d_{v0} \{a_{3,j}^2 + b_{3,j}^2\}] \\ & + \frac{L}{\pi j} \left[2 \left(1 - \frac{2\pi\delta_m j}{L} \right) \{a_{2,j}^2 + b_{2,j}^2\} \right. \\ & \quad + \frac{1}{2} \{a_{1,j}^2 + a_{3,j}^2 + b_{1,j}^2 + b_{3,j}^2\} \\ & \quad - 2 \{a_{1,j}a_{2,j} + a_{2,j}a_{3,j} + b_{1,j}b_{2,j} + b_{2,j}b_{3,j}\} e^{-2\pi\delta_m j/L} \\ & \quad \left. + \{a_{1,j}a_{3,j} + b_{1,j}b_{3,j}\} e^{-4\pi\delta_m j/L} \right]. \end{aligned}$$

Proof. Analogous to the proof of Theorem 3.6. □

4 Stability

In this section we study stability of monolayers and bilayers with respect to the admissible perturbations. The bilayer will be treated in Section 4.2, the monolayer in Section 4.3.

4.1 Preliminary definitions and results

In this paper we only consider *linear* stability—whenever we use the words *stable* or *unstable*, this refers to the sign of the second derivative:

Definition 4.1. *Using the notation of Section 3, the VUV bilayer (monolayer) of optimal width (u_0, v_0) is called stable iff*

$$\left. \frac{d^2}{d\varepsilon^2} \mathcal{F}(u_\varepsilon, v_\varepsilon) \right|_{\varepsilon=0} \geq 0,$$

for every $p \in \mathcal{P}_b^M$ (\mathcal{P}_m^M), and unstable otherwise.

The following property simplifies the study of stability of the bilayers and monolayers.

Lemma 4.2. *Using the notation from Theorem 3.6 we have, for any $x, y \in \mathbb{R}^4$ and for $j \geq 1$,*

$$\begin{aligned} B_j(x, y, d_{uv}, d_{v0}, L) &= B_1(x, y, d_{uv}, d_{v0}, L/j), \\ B_j(x, 0, d_{uv}, d_{v0}, L) &= B_j(0, x, d_{uv}, d_{v0}, L), \\ B_j(x, y, d_{uv}, d_{v0}, L) &= B_j(x, 0, d_{uv}, d_{v0}, L) + B_j(0, y, d_{uv}, d_{v0}, L). \end{aligned}$$

Similarly, in the notation from Theorem 3.10 we have, for any $x, y \in \mathbb{R}^3$ and for $j \geq 1$,

$$\begin{aligned} M_j(x, y, d_{u0}, d_{uv}, d_{v0}, L) &= M_1(x, y, d_{u0}, d_{uv}, d_{v0}, L/j), \\ M_j(x, 0, d_{u0}, d_{uv}, d_{v0}, L) &= M_j(0, x, d_{u0}, d_{uv}, d_{v0}, L), \\ M_j(x, y, d_{u0}, d_{uv}, d_{v0}, L) &= M_j(x, 0, d_{u0}, d_{uv}, d_{v0}, L) + M_j(0, y, d_{u0}, d_{uv}, d_{v0}, L). \end{aligned}$$

Proof. These properties follow from the definitions of B_j in Theorem 3.6 and M_j in Theorem 3.10. \square

4.2 Stability of the bilayer

Throughout this subsection we will use the notation as introduced in Section 3.2. Lemma 4.2 provides us with a simpler characterisation of stability:

Corollary 4.3. *The VUV bilayer is stable iff*

1. $B_0(\mathbf{a}_0, \delta_b) \geq 0$ for all $\mathbf{a}_0 \in \mathbb{R}^4$ satisfying (15), and
2. $B_1(x, 0, d_{uv}, d_{v0}, L/j) \geq 0$ for all $x \in \mathbb{R}^4$ and all $j \geq 1$.

We therefore study B_0 and B_1 as quadratic forms on \mathbb{R}^4 subject to (15) and investigate their sign. Note that B_0 and B_1 can be identified with symmetric 4×4 matrices, and we will continuously make this identification. Among other things that means we can speak of eigenvalues of B_0 and B_1 , and relate the sign of the quadratic forms to the signs of their eigenvalues.

Lemma 4.4. $B_0(\mathbf{a}, \delta_b) \geq 0$ for all $\delta_b > 0$ and for all $\mathbf{a}_0 \in \mathbb{R}^4$ satisfying (15).

Proof. The Lemma follows immediately from writing B_0 as

$$\frac{1}{4\delta_b} B_0(\mathbf{a}_0, \delta_b) = -\frac{1}{2} (2a_{1,0} - a_{2,0} + 2a_{3,0} - a_{4,0})^2 + \frac{1}{2} (a_{1,0} - a_{2,0} - a_{3,0} + a_{4,0})^2 + \frac{1}{2} (a_{1,0} + a_{3,0})^2.$$

\square

Lemma 4.5. *Two of the four eigenvalues of B_1 are nonnegative for all d_{uv}, d_{v0} , and L ; the other two do not have a definite sign. Denote the smallest eigenvalue by $\lambda_1^b(d_{uv}, d_{v0}, L)$. Define*

$$v := e^{-2\pi\delta_b/L}, \quad \zeta := \frac{d_{uv}}{d_{uv} + d_{v0}} = \frac{c_u + c_v}{c_0 + c_u + 2c_v}. \quad (20)$$

There exists a function $\zeta_1 \in C([0, 1])$ (see (23)) such that

$$\lambda_1^b(d_{uv}, d_{v0}, L) \geq 0 \iff \zeta \geq \zeta_1(v).$$

Proof. Note that $v \in (0, 1)$ and, by conditions (3), $\zeta \in \left[\frac{1}{2} - \frac{c_u + c_0}{2(c_0 + c_u + 2c_v)}, \frac{1}{2} + \frac{c_u + c_0}{2(c_0 + c_u + 2c_v)} \right] \subset [0, 1]$. Let $x \in \mathbb{R}^4$. We now write

$$B_1(x, 0, d_{uv}, d_{v0}, L) = \frac{2L}{\pi} \tilde{B}_1(x, \zeta, v),$$

where

$$\begin{aligned}\tilde{B}_1(x, \zeta, v) &:= -\frac{1}{3} \log^3 v \left(\zeta (x_1^2 + x_3^2) + (1 - \zeta) (x_2^2 + x_4^2) \right) \\ &\quad + (1 + \log v) (x_1^2 + x_3^2) + \frac{1}{4} (x_2^2 + x_4^2) \\ &\quad - (x_1 x_2 + x_3 x_4) v + 2x_1 x_3 v^2 - (x_1 x_4 + x_2 x_3) v^3 + \frac{1}{2} x_2 x_4 v^4.\end{aligned}\tag{21}$$

Note that when $x_1 = x_3 = 0$,

$$\tilde{B}_1(x, \zeta, v) = (1 - \zeta) (x_2^2 + x_4^2) + \frac{1}{4} (x_2^2 + x_4^2) + \frac{1}{2} x_2 x_4 v^4 \geq 0,$$

so that by the max-min characterisation of the third eigenvalue λ_3^b , for fixed ζ, v , we have

$$\lambda_3^b = \max_{\dim L=2} \min_{\substack{x \in \mathbb{R}^4/L \\ |x|=1}} \tilde{B}_1(x, \zeta, v) \geq \min_{\substack{x_1=x_3=0 \\ |x|=1}} \tilde{B}_1(x, \zeta, v) \geq 0,$$

implying that the largest two eigenvalues are always non-negative.

We now turn to the question of existence of admissible x such that \tilde{B}_1 is negative, and we simplify the problem by minimizing \tilde{B}_1 with respect to x_2 and x_4 under fixed x_1 and x_3 . The stationarity conditions $\frac{\partial}{\partial x_2} \tilde{B}_1(x, \zeta, v) = 0$ and $\frac{\partial}{\partial x_4} \tilde{B}_1(x, \zeta, v) = 0$ lead to the equations

$$\begin{pmatrix} x_2^{\text{opt}} \\ x_4^{\text{opt}} \end{pmatrix} = \frac{1}{\det A(\zeta, v)} A(\zeta, v) \begin{pmatrix} v & v^3 \\ v^3 & v \end{pmatrix} \begin{pmatrix} x_1 \\ x_3 \end{pmatrix},$$

where

$$A(\zeta, v) := \begin{pmatrix} \frac{1}{2} - \frac{2}{3}(1 - \zeta) \log^3 v & -\frac{1}{2} v^4 \\ -\frac{1}{2} v^4 & \frac{1}{2} - \frac{2}{3}(1 - \zeta) \log^3 v \end{pmatrix}.$$

Inserting these results into \tilde{B}_1 gives

$$\tilde{B}_1(x_1, x_2^{\text{opt}}, x_3, x_4^{\text{opt}}, \zeta, v) = (x_1, x_3) \overset{\times}{B}(\zeta, v) (x_1, x_3)^T,$$

where the matrix entries of $\overset{\times}{B}$ are given by

$$\begin{aligned}\overset{\times}{B}_{11}(\zeta, v) &= \overset{\times}{B}_{22}(\zeta, v) = \log v - \frac{1}{3} \zeta \log^3 v \\ &\quad - \frac{\left(3(-1 + v^2) - 4(-1 + \zeta) \log^3 v \right) \left(3(-1 + v^6) - 4(-1 + \zeta) \log^3 v \right)}{9(-1 + v^8) + 8(-1 + \zeta) \left(-3 - 2(-1 + \zeta) \log^3 v \right) \log^3 v}, \\ \overset{\times}{B}_{12}(\zeta, v) &= \overset{\times}{B}_{21}(\zeta, v) = -\frac{\left(3v(-1 + v^2) - 4v(-1 + \zeta) \log^3 v \right)^2}{9(-1 + v^8) + 8(-1 + \zeta) \left(-3 - 2(-1 + \zeta) \log^3 v \right) \log^3 v}.\end{aligned}$$

The eigenvalues of $\overset{\times}{B}$ are

$$\begin{aligned}G_-(\zeta, v) &:= 1 - v^2 + \log v - \frac{1}{3} \zeta \log^3 v + \frac{3v^2(-1 + v^2)^2}{3(-1 + v^4) - 4(-1 + \zeta) \log^3 v} \\ &= \left(3(-1 + v^4) - 4(-1 + \zeta) \log^3 v \right)^{-1} h_-(\zeta, v), \\ G_+(\zeta, v) &:= 1 + v^2 + \log v - \frac{1}{3} \zeta \log^3 v - \frac{3v^2(1 + v^2)^2}{3(1 + v^4) + 4(-1 + \zeta) \log^3 v} \\ &= \left(3(1 + v^4) + 4(-1 + \zeta) \log^3 v \right)^{-1} h_+(\zeta, v),\end{aligned}$$

with

$$\begin{aligned}
h_-(\zeta, v) &:= \left(\frac{4}{3} \log^6 v\right) \zeta^2 + \left(-\frac{4}{3} \log^6 v - 4 \log^4 v + (-3 + 4v^2 - v^4) \log^3 v\right) \zeta \\
&\quad - 3(1 - v^2)^2 + 3(-1 + v^4) \log v + 4(1 - v^2) \log^3 v + 4 \log^4 v, \\
h_+(\zeta, v) &:= -\left(\frac{4}{3} \log^6 v\right) \zeta^2 + \left(\frac{4}{3} \log^6 v + 4 \log^4 v + (3 + 4v^2 - v^4) \log^3 v\right) \zeta \\
&\quad + 3(1 - v^4) + 3(1 + v^4) \log v - 4(1 + v^2) \log^3 v - 4 \log^4 v.
\end{aligned}$$

Note that $G_- < G_+$, since for $v \in (0, 1), \zeta \in [0, 1]$,

$$3(1 + v^4) + 4(-1 + \zeta) \log^3 v > 0, \quad 3(-1 + v^4) - 4(-1 + \zeta) \log^3 v < 0,$$

and thus

$$G_+(\zeta, v) - G_-(\zeta, v) = \frac{-2v^2 \left(3(-1 + v^2) - 4(-1 + \zeta) \log^3 v\right)^2}{\left(3(1 + v^4) + 4(-1 + \zeta) \log^3 v\right) \left(3(-1 + v^4) - 4(-1 + \zeta) \log^3 v\right)} > 0.$$

We have now the following equivalences:

$$\begin{aligned}
\forall x \in \mathbb{R}^4, B_1(x, 0, d_{uv}, d_{v0}, L) \geq 0 &\iff \forall x \in \mathbb{R}^4, \tilde{B}_1(x, \zeta, v) \geq 0 \\
&\iff \overset{\star}{\tilde{B}}(\zeta, v) \geq 0 \\
&\iff G_-(\zeta, v) \geq 0.
\end{aligned}$$

We prove the following characterisation of the sign of G_- :

$$G_-(\zeta, v) \geq 0 \iff \zeta \geq \zeta_1(v), \quad (22)$$

where

$$\begin{aligned}
\zeta_1(v) &= (8 \log^3 v)^{-1} \left(9 - 12v^2 + 3v^4 + (4 \log v)(3 + \log^2 v) \right. \\
&\quad \left. + \left\{ 225 - 504v^2 + 342v^4 - 72v^6 + 9v^8 + (360 - 288v^2 - 72v^4) \log v \right. \right. \\
&\quad \left. \left. + 144 \log^2 v + (-120 + 96v^2 + 24v^4) \log^3 v - 96 \log^4 v + 16 \log^6 v \right\}^{\frac{1}{2}} \right). \quad (23)
\end{aligned}$$

The details of this calculation can be found in Appendix D. This concludes the proof. \square

The function g_1 mentioned in Theorem 1.2 in the introduction is related to ζ_1 , given in (23), by

$$g_1(\ell) := \zeta_1(e^{2\pi/\ell}). \quad (24)$$

Remark 4.6. The four eigenvalues of \tilde{B}_1 from the proof of Lemma 4.5 are

$$\begin{aligned}
&\frac{1}{72} \left(45 - 36v^2 - 9v^2 + 36 \log v - 12 \log^3 v \right. \\
&\quad \left. \pm \left\{ (-45 + 36v^2 + 9v^4 - 36 \log v + 12 \log^3 v)^2 \right. \right. \\
&\quad \left. \left. - 144 \left(9 - 18v^2 + 9v^4 + 9 \log v - 9v^4 \log v - 12 \log^3 v + 12v^2 \log^3 v + 9\zeta \log^3 v \right. \right. \right. \\
&\quad \left. \left. \left. - 12v^2 \zeta \log^3 v + 3v^4 \zeta \log^3 v - 12 \log v^4 + 12\zeta \log^4 v + 4\zeta \log^6 v - 4\zeta^2 \log^6 v \right) \right\}^{\frac{1}{2}} \right),
\end{aligned}$$

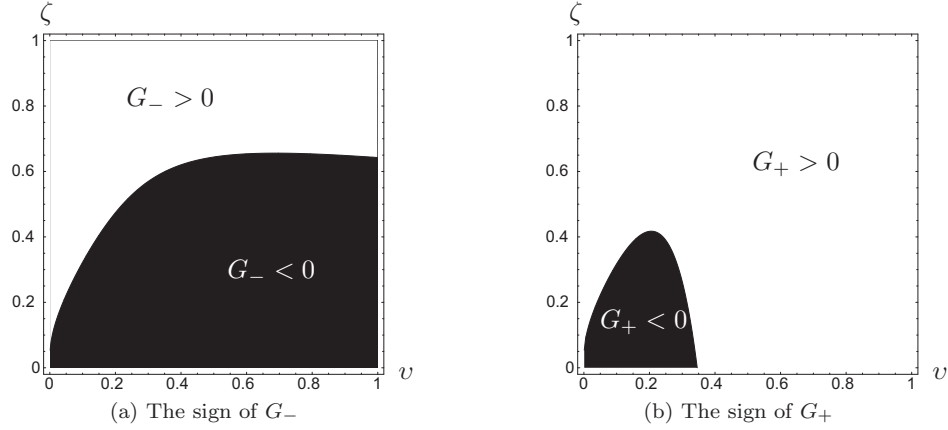


Figure 10: The sign in parameter space of the eigenvalues $G_- < G_+$. The boundary between the two regions in the left-hand figure is given by $\zeta = \zeta_1(v)$.

and

$$\begin{aligned} & \frac{1}{72} \left(45 + 36v^2 + 9v^4 + 36 \log v - 12 \log^3 v \right. \\ & \quad \pm \left\{ \left(45 + 36v^2 + 9v^4 + 36 \log v - 12 \log^3 v \right)^2 \right. \\ & \quad \quad \left. + 144 \left(-9 + 9v^4 - 9 \log v - 9v^4 \log v + 12 \log^3 v + 12v^2 \log^3 v - 9\zeta \log^3 v \right. \right. \\ & \quad \quad \quad \left. \left. - 12v^2 \zeta \log^3 v + 3v^4 \zeta \log^3 v + 12 \log v^4 - 12\zeta \log^4 v - 4\zeta \log^6 v + 4\zeta^2 \log^6 v \right) \right\}^{\frac{1}{2}} \Big). \end{aligned}$$

Plotting the areas where these eigenvalues are negative shows that the eigenvalues with the plus sign chosen for \pm are positive everywhere for $v \in (0, 1)$ and $\zeta \in [0, 1]$. The plots for the other two eigenvalues correspond with those in Figure 10.

Collecting Lemmas 4.4 and 4.5 we can summarise the stability properties with the use of Corollary 4.3 as follows:

Theorem 4.7. *Let ζ , v , and ζ_1 be as in Lemma 4.5. Define the functions $\underline{\zeta}_j$, $j \geq 1$, and $\tilde{\zeta}$ by*

$$\underline{\zeta}_j(v) := \zeta_1(v^j), \quad \tilde{\zeta}(v) := \sup_{j \geq 1} \underline{\zeta}_j(v).$$

Then the VUV bilayer of optimal width (6) is stable with respect to all (mass-conserving) perturbations in \mathcal{P}_b^M iff

$$\zeta \geq \tilde{\zeta}(v).$$

This is Theorem 1.2 from the introduction. Its implications are illustrated in Figure 4b.

Remark 4.8. Note that the statement in Theorem 4.7 about the positivity of the second variation also holds true if we allow the perturbations to come from the larger set of perturbations \mathcal{P}_b , instead of \mathcal{P}_b^M . However, as stated in Remark 3.2, the bilayer of optimal width is not stationary under perturbations that do not preserve mass.

We next show that $\tilde{\zeta}$ is bounded from above away from 1. Therefore there is a threshold α (as mentioned in the introduction) such that the bilayer is stable if $\zeta \geq \alpha$.

Lemma 4.9. *Let $\tilde{\zeta}$ be as in Theorem 4.7, then there exists $\alpha \in (0, 1)$ such that for all $v \in (0, 1)$,*

$$\tilde{\zeta}(v) < \alpha < 1.$$

Proof. First note that per definition of $\tilde{\zeta}$ it suffices to show that there exists a $c \in (0, 1)$, such that for all $v \in (0, 1)$,

$$\zeta_1(v) < c < 1.$$

Since ζ_1 is continuous on the interval $(0, 1)$ and goes to zero for $v \downarrow 0$ and to $\frac{5}{2} - \frac{1}{2}\sqrt{\frac{69}{5}}$ for $v \uparrow 1$ (see Remark D.1), this is equivalent to

$$(8 \log^3 v)(\zeta_1(v) - 1) > 0.$$

By (40) we know that

$$\begin{aligned} 0 &< \left((9 - 12v^2 + 3v^4 + (4 \log v)(3 + \log^2 v)) - 8 \log^3 v \right)^2 \\ &< 225 - 504v^2 + 342v^4 - 72v^6 + 9v^8 + (360 - 288v^2 - 72v^4) \log v \\ &\quad + 144 \log^2 v + (-120 + 96v^2 + 24v^4) \log^3 v - 96 \log^4 v + 16 \log^6 v. \end{aligned}$$

Taking square roots completes the proof. \square

Remark 4.10. To find out the stable and unstable first-order Fourier modes of deformation for the bilayer, we compute the eigenvectors belonging to the positive and (potentially) negative eigenvalues of \tilde{B}_1 from (21). For the stable directions we find

$$\begin{aligned} \mathbf{a}_1^{s1}(\zeta, v) &:= \left(\frac{1}{12v(1+v^2)} \left(f_1(\zeta, v) - \sqrt{f_4(\zeta, v)} \right), 1, \frac{2}{v} \frac{f_2(\zeta, v) - \sqrt{f_4(\zeta, v)}}{f_3(\zeta, v) + \sqrt{f_4(\zeta, v)}}, 1 \right), \\ \mathbf{a}_1^{s2}(\zeta, v) &:= \left(\frac{1}{12v(-1+v^2)} \left(g_1(\zeta, v) - \sqrt{g_4(\zeta, v)} \right), -1, \frac{2}{v} \frac{g_2(\zeta, v) + \sqrt{g_4(\zeta, v)}}{g_3(\zeta, v) - \sqrt{g_4(\zeta, v)}}, 1 \right), \end{aligned}$$

where

$$\begin{aligned} f_1(\zeta, v) &:= -9 - 12v^2 + 3v^4 - 12 \log v + (-4 + 8\zeta) \log^3 v \\ f_2(\zeta, v) &:= -9 - 3v^2(6 + v^2) - 12 \log v + (-4 + 8\zeta) \log^3 v \\ f_3(\zeta, v) &:= 15 + 3v^2(4 + v^2) - 12 \log v + (-4 + 8\zeta) \log^3 v \\ f_4(\zeta, v) &:= 9(9 + 40v^2 + 42v^4 + 8v^6 + v^8) \\ &\quad + 8 \log v \left(-3 + (-1 + 2\zeta) \log^2 v \right) \left(3(-3 - 4v^2 + v^4) - 6 \log v + (-2 + 4\zeta) \log^3 v \right), \\ g_1(\zeta, v) &:= -9 + 12v^2 - 3v^4 - 12 \log v + (-4 + 8\zeta) \log^3 v \\ g_2(\zeta, v) &:= 9 - 3v^2(2 + v^2) + 12 \log v + (4 - 8\zeta) \log^3 v \\ g_3(\zeta, v) &:= -15 + 3v^2(4 + v^2) + 12 \log v + (4 - 8\zeta) \log^3 v \\ g_4(\zeta, v) &:= 9(-1 + v^2)^2(1 + v^2)(9 + v^2) \\ &\quad + 8 \log v \left(-3 + (-1 + 2\zeta) \log^2 v \right) \left(-3(3 - 4v^2 + v^4) - 6 \log v + (-2 + 4\zeta) \log^3 v \right). \end{aligned}$$

The directions belonging to the eigenvalues that can become negative, corresponding to the eigenvalues G_+ and G_- of the reduced matrix \tilde{B} in the proof of Lemma 4.5, are

$$\begin{aligned} \mathbf{a}_1^{u1}(\zeta, v) &:= \left(\frac{1}{12v(1+v^2)} \left(f_1(\zeta, v) + \sqrt{f_4(\zeta, v)} \right), 1, \frac{2}{v} \frac{f_2(\zeta, v) + \sqrt{f_4(\zeta, v)}}{f_3(\zeta, v) - \sqrt{f_4(\zeta, v)}}, 1 \right), \\ \mathbf{a}_1^{u2}(\zeta, v) &:= \left(\frac{1}{12v(-1+v^2)} \left(g_1(\zeta, v) + \sqrt{g_4(\zeta, v)} \right), -1, \frac{2}{v} \frac{g_2(\zeta, v) + \sqrt{g_4(\zeta, v)}}{g_3(\zeta, v) + \sqrt{g_4(\zeta, v)}}, 1 \right), \end{aligned}$$

respectively.

The direction of the perturbation \mathbf{a}_1^{u1} is depicted in Figure 7a. Here we have chosen the values $d_{uv} = 0.7$, $d_{v0} = 0.3$, $L = 5$ and $\varepsilon = 0.25$. Similarly we get Figures 7b, 7c, and 7d using perturbations \mathbf{a}_1^{u2} , \mathbf{a}_1^{s1} , and \mathbf{a}_1^{s2} respectively.

4.3 Stability of the monolayer

We now redo the arguments for the monolayer of optimal width (16). Throughout this subsection we use the notation of Section 3.3.

We can simplify M_1 a bit by writing

$$\nu := e^{-2\pi\delta_m/L}, \quad \varrho := \frac{d_{u0}}{d_{u0} + d_{uv} + d_{v0}} = \frac{c_u + c_0}{2(c_0 + c_u + c_v)}, \quad \varsigma := \frac{d_{v0}}{d_{u0} + d_{uv} + d_{v0}} = \frac{c_v + c_0}{2(c_0 + c_u + c_v)}.$$

Note the slightly different definition of ν than for the bilayer (20). Then, for all $x \in \mathbb{R}^3$,

$$M_1(x, 0, d_{u0}, d_{uv}, d_{v0}, L) = \frac{L}{\pi} \tilde{M}_1(x, \varrho, \varsigma, \nu),$$

where

$$\begin{aligned} \tilde{M}_1(x, \varrho, \varsigma, \nu) := & -\frac{2}{3} \log^3 \nu (\varrho x_1^2 + (1 - \varrho - \varsigma)x_2^2 + \varsigma x_3^2) \\ & + 2(1 + \log \nu)x_2^2 + \frac{1}{2}(x_1^2 + x_3^2) \\ & - 2(x_1 + x_3 + x_2x_3)\nu + x_1x_3\nu^2. \end{aligned}$$

We now can write

$$\tilde{M}_1(x, \varrho, \varsigma, \nu) = x^T \hat{M}(\varrho, \varsigma, \nu) x,$$

with

$$\hat{M}(\varrho, \varsigma, \nu) := \begin{pmatrix} -\frac{2}{3}\varrho \log^3 \nu + \frac{1}{2} & & -\nu & & \frac{1}{2}\nu^2 \\ & -\nu & & -\frac{2}{3}(1 - \varrho - \varsigma) \log^3 \nu + 2(1 + \log \nu) & -\nu \\ & \frac{1}{2}\nu^2 & & -\nu & -\frac{2}{3}\varsigma \log^3 \nu + \frac{1}{2} \end{pmatrix}.$$

This matrix is well defined for all $\varrho, \varsigma \in \mathbb{R}$, $\nu > 0$, but note that the nonnegativity of the parameters c_0 , c_u , and c_v —or equivalently conditions (3)—translates into

$$0 \leq \varrho \leq \frac{1}{2}, \quad 0 \leq \varsigma \leq \frac{1}{2}, \quad \varrho + \varsigma \geq \frac{1}{2}, \quad (25)$$

and furthermore $\nu \in (0, 1)$ by definition.

Remark 4.11. As explained in the introduction and Appendix B, we assume throughout the paper that for the monolayer the interfaces U-0 and V-0 are penalised equally strongly, i.e. $d_{u0} = d_{v0}$ or equivalently $c_u = c_v$. Under this assumption $\chi = \kappa$, and the inequalities in (25) imply that χ and κ take values in $[\frac{1}{4}, \frac{1}{2}]$.

Lemma 4.12. *Let $c_u = c_v$. Two of the three eigenvalues of $\hat{M}(\varsigma, \nu)$ are nonnegative for all $\nu \in (0, 1)$ and $\varsigma \in [\frac{1}{4}, \frac{1}{2}]$. The third eigenvalue is given by*

$$E_3(\varsigma, \nu) := \frac{1}{12} \left(e_1(\varsigma, \nu) - \sqrt{e_2(\varsigma, \nu)} \right),$$

where $\nu \in (0, 1)$, $\varsigma \in [\frac{1}{4}, \frac{1}{2}]$ and e_1 and e_2 are given in (27) and (28). The sign of E_3 is characterised by

$$E_3(\varsigma, \nu) \geq 0 \iff \varsigma \leq \varsigma_2(\nu) \quad (26)$$

with ς_2 as given in (29).

Proof. Since we are interested in the case where $c_u = c_v$ we will take $\varrho = \varsigma$ from here on, which turns the conditions (25) into $\frac{1}{4} \leq \varsigma \leq \frac{1}{2}$. For the three eigenvalues of $M_1(\varsigma, \varsigma, \nu)$ we compute

$$\begin{aligned} E_1(\varsigma, \nu) &:= \frac{1}{6}(3 - 3\nu^2 - 4\varsigma \log^3 \nu), \\ E_{2,3}(\varsigma, \nu) &:= \frac{1}{12} \left(e_1(\varsigma, \nu) \pm \sqrt{e_2(\varsigma, \nu)} \right), \end{aligned}$$

where

$$\begin{aligned} e_1(\varsigma, \nu) &:= 15 + 3\nu^2 + (12 - 4 \log^2 \nu + 4\varsigma \log^2 \nu) \log \nu, & (27) \\ e_2(\varsigma, \nu) &:= 81 + 234\nu^2 + 9\nu^4 + 216 \log \nu - 72\nu^2 \log \nu + 144 \log^2 \nu \\ &\quad - 72 \log^3 \nu + 24\nu^2 \log^3 \nu - 96 \log^4 \nu + 16 \log^6 \nu \\ &\quad + (216 \log^3 \nu - 72\nu^2 \log^3 \nu + 288 \log^4 \nu - 96 \log^6 \nu) \varsigma \\ &\quad + (144 \log^6 \nu) \varsigma^2 & (28) \end{aligned}$$

and we choose the plus sign for E_2 and the minus sign for E_3 .

First note that $\nu \in (0, 1)$ and $\chi \geq 0$ imply that E_1 is always positive. $E_{2,3}$ are real, since they are the eigenvalues of a symmetric matrix and thus $e_2(\varsigma, \nu) \geq 0$ for all $\varsigma \in \mathbb{R}$ and for all $\nu \in (0, 1)$.

Since for all $x > 0$ and $\chi \leq 1/2$ we have $(1 - \chi)x^3 - 3x \geq (1/2)x^3 - 3x \geq -2\sqrt{2}$,

$$e_1(\varsigma, \nu) = 15 + 3\nu^2 + 4[(1 - \chi)|\log \nu|^3 - 3|\log \nu|] \geq 15 - 8\sqrt{2} > 0.$$

Combining this result with $e_2(\varsigma, \nu) \geq 0$, we conclude that $E_2(\varsigma, \nu) > 0$ for all admissible ς, ν . Thus, the only eigenvalue that might be negative (in all or part of parameter space) is E_3 .

To prove the statements in (26) we compute

$$\begin{aligned} \frac{1}{16} \left(e_1^2(\varsigma, \nu) - e_2(\varsigma, \nu) \right) &= 9(1 - \nu^2) + 9(1 + \nu^2) \log \nu - 3(1 + \nu^2) \log^3 \nu \\ &\quad + \left(6(-1 + \nu^2) \log^3 \nu + 4(-3 + \log^2 \nu) \log^4 \nu \right) \varsigma \\ &\quad - (8 \log^6 \nu) \varsigma^2. \end{aligned}$$

This expression is negative on $(0, 1)$ if and only if $\varsigma \in [\frac{1}{4}, \varsigma_1(\nu)) \cup (\varsigma_2(\nu), \frac{1}{2}]$ and zero if and only if $\varsigma = \varsigma_1(\nu)$ or $\varsigma = \varsigma_2(\nu)$, where

$$\varsigma_{1,2}(\nu) := \frac{1}{16 \log^6 \nu} \left(f(\nu) \pm \sqrt{g(\nu)} \right), \quad (29)$$

with

$$\begin{aligned} f(\nu) &:= \left(6(-1 + \nu^2) + 4(-3 + \log^2 \nu) \log \nu \right) \log^3 \nu; \\ g(\nu) &:= 96 \log^6 \nu \left(3(1 - \nu^2) + 3(1 + \nu^2) \log \nu - (1 + \nu^2) \log^3 \nu \right) \\ &\quad + \left(6(-1 + \nu^2) \log^3 \nu + 4(\log^2 \nu - 3) \log^4 \nu \right)^2. \end{aligned}$$

The minus sign is chosen in ς_1 while in ς_2 we choose the plus sign. Plots of ς_1 and ς_2 are shown in Figure 11.

It is left to prove now that $\varsigma_1(\nu) < 1/4$ for all $\nu \in (0, 1)$. We will actually prove the stronger statement $\varsigma_1(\nu) < 0$, which follows from

$$\begin{aligned} &g(\nu) > 0 && \text{for } 0 < \nu < 1, \\ \iff &f(\nu)^2 - g(\nu) < 0 && \text{for } 0 < \nu < 1, \\ \iff &3(1 - \nu^2) + 3(1 + \nu^2) \log \nu - (1 + \nu^2) \log^3 \nu > 0 && \text{for } 0 < \nu < 1, \\ \iff &3 \frac{1 - \nu^2}{1 + \nu^2} + 3 \log \nu - \log^3 \nu > 0 && \text{for } 0 < \nu < 1, \\ \stackrel{w = -\log \nu}{\iff} &3 \tanh w - 3w + w^3 > 0 && \text{for } w > 0. \end{aligned}$$

To prove that this last inequality holds, we define $h(w) := \tanh w - 3w + w^3$ and use $\tanh' w = 1 - \tanh^2 w$, to compute that $h'''(w) = 6 \tanh^2 w (-3 \tanh^4 w + 4) > 0$. From this it follows by integration that $h(w) > 0$ for all $w > 0$. \square

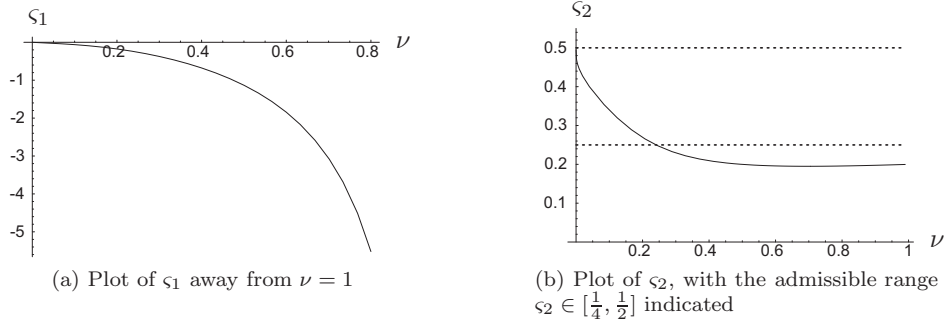


Figure 11:

Remark 4.13. For the excluded endpoints 0 and 1 we find

$$\begin{aligned} \lim_{\nu \downarrow 0} \varsigma_1 &= 0, & \lim_{\nu \uparrow 1} \varsigma_1 &= -\infty, \\ \lim_{\nu \downarrow 0} \varsigma_2 &= \frac{1}{2}, & \lim_{\nu \uparrow 1} \varsigma_2 &= \frac{1}{5}. \end{aligned}$$

The limits for $\nu \uparrow 1$ were found by calculating the first terms in the Taylor expansion of $\varsigma_{1,2}$.

Figure 12 shows the parts of parameter space where E_3 is positive and negative, both on the admissible domain $(\frac{1}{4}, \frac{1}{2})$ for ς as well as extended to $(0, 1)$.

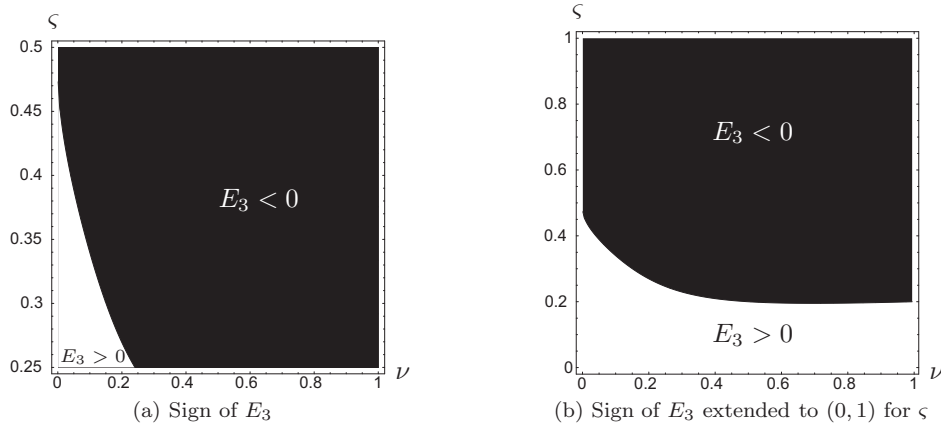


Figure 12:

Remark 4.14. Expanding E_3 around $\nu = 1$ gives

$$E_3(\varsigma, \nu) = \frac{4}{45}(1 - 5\varsigma)(1 - \nu)^5 + \mathcal{O}\left((1 - \nu)^6\right),$$

for $\nu \uparrow 1$. Since $1 - 5\varsigma \leq -\frac{1}{4}$ for $\varsigma \in [\frac{1}{4}, \frac{1}{2}]$ we can conclude that for ν close to 1 (or equivalently large L) the monolayer is unstable for all admissible values for the interfacial (surface tensions) coefficients d_{ij} (or c_i). This corresponds to what is shown in Figure 12a.

Taking into account the assumption $d_{v0} = d_{u0}$, the condition $1 - 5\varsigma < 0$ for negativity of E_3 is equivalent to $d_{uv} < \frac{3}{2}(d_{u0} + d_{v0})$. In [17, Theorem 8] we show that for a circular two-dimensional

monolayer the term in the energy per unit mass \mathcal{F}/M that is quadratic in the curvature is given by

$$m \left(-\frac{1}{2}(d_{u0} + d_{v0}) + \frac{4}{15}m^3 \right) \kappa^2,$$

where m is the thickness of the layers and κ is the curvature. Taking $m = \delta_m$ we find that this term becomes negative exactly as $d_{uv} < \frac{3}{2}(d_{u0} + d_{v0})$, showing that the (large) circular monolayer loses stability at the same point as the flat monolayer on large domains. Note that conditions (3) imply $d_{uv} < \frac{3}{2}(d_{u0} + d_{v0})$.

In order to compare the results for the monolayer to those for the bilayer, we introduce the relative U-V interface penalisation

$$\mu := 1 - \varrho - \varsigma = \frac{c_u + c_v}{2(c_0 + c_u + c_v)}, \quad (30)$$

analogous to ζ for the bilayer in Lemma 4.5. Note that conditions (3) give $\mu \in [0, \frac{1}{2}]$. In terms of the surface tension coefficients,

$$\mu = \frac{d_{uv}}{d_{u0} + d_{uv} + d_{v0}},$$

μ is interpreted as the relative penalisation of the U-V interface.

Theorem 4.15. *Let $d_{u0} = d_{v0}$ and let ς_2 be as in Lemma 4.12. Define the functions $\underline{\varsigma}_j$ and $\tilde{\varsigma}$ by*

$$\underline{\varsigma}_j(\nu) := \varsigma_2(\nu^j), \quad \tilde{\varsigma} := \inf_{j \geq 1} \underline{\varsigma}_j, \quad \tilde{\mu} := 1 - 2\tilde{\varsigma}.$$

The monolayer of optimal width (16) is stable with respect to perturbations in \mathcal{P}_m^M if and only if $\mu \geq \tilde{\mu}(\nu)$.

Proof. First we work with ς as in Lemma 4.12 and afterwards we translate the results into conditions on μ . By Definition 4.1 and Theorem 3.10 in order to prove stability, we have to prove that

$$M_0(\mathbf{a}_0, \delta_m) + \sum_{j=1}^{\infty} M_j(\mathbf{a}_j, \mathbf{b}_j, d_{u0}, d_{uv}, d_{v0}, L) \geq 0,$$

for all admissible perturbations. Per definition we have $M_0(\mathbf{a}_0, \delta_m) := \delta_m (a_{1,0} - a_{3,0})^2 \geq 0$. By Lemma 4.12 we know that if (ν, ς) is such that $\varsigma \in [\frac{1}{4}, \varsigma_2(\nu)]$ then $M_1(\mathbf{a}_1, 0, d_{u0}, d_{uv}, d_{v0}, L) \geq 0$ for all $p \in \mathcal{P}_m$. By Lemma 4.2 we have for $j \geq 1$,

$$\forall \mathbf{a}_j, \mathbf{b}_j, M_j(\mathbf{a}_j, \mathbf{b}_j, d_{u0}, d_{uv}, d_{v0}, L) \geq 0 \iff \forall \mathbf{a}_1, M_1(\mathbf{a}_1, 0, d_{u0}, d_{uv}, d_{v0}, L/j) \geq 0,$$

thus we see that, if $\varsigma \in [\frac{1}{4}, \tilde{\varsigma}(\nu)]$ is satisfied, then for all $j \geq 1$, for all \mathbf{a}_j , and for all \mathbf{b}_j , $M_j(\mathbf{a}_j, \mathbf{b}_j, d_{u0}, d_{uv}, d_{v0}, L) \geq 0$.

Now note that $\varsigma = \frac{1-\mu}{2}$ and thus

$$\varsigma \in \left[\frac{1}{4}, \tilde{\varsigma}(\nu) \right] \iff \mu \in \left[1 - 2\tilde{\varsigma}(\nu), \frac{1}{2} \right],$$

which proves the statement of the theorem. \square

To make the connection to Theorem 1.1 in the introduction, the function f_1 is defined by

$$f_1(\ell) := 1 - 2\chi_2 \left(e^{2\pi/\ell} \right), \quad (31)$$

where χ_2 is given in (29).

Figure 4a illustrates the stability properties of the monolayer of optimal width from Theorem 4.15.

Remark 4.16. In Theorem 4.15 we only consider perturbations in \mathcal{P}_m^M , i.e. perturbations that keep the total mass fixed. The statement about the positivity of the second variation still holds if we consider the larger set of perturbations \mathcal{P}_m , however, for these perturbations the monolayer of optimal width is not a stationary point, as was noted after Lemma 3.8.

Remark 4.17. To find the stable and unstable first order Fourier modes of deformation we compute the eigenvectors belonging to the positive eigenvalues of $\tilde{M}_1(\mathbf{a}_1, \varsigma, \nu)$ and to the eigenvalues that are negative for some parameter choices. For the positive, stable directions we find

$$\begin{aligned}\mathbf{a}_1^{s_1}(\varsigma, \nu) &:= (-1, 0, 1), \\ \mathbf{a}_1^{s_2}(\varsigma, \nu) &:= \left(1, \frac{1}{12\nu} \left(h_1(\varsigma, \nu) + \sqrt{h_2(\varsigma, \nu)}\right), 1\right),\end{aligned}$$

where

$$\begin{aligned}h_1(\varsigma, \nu) &:= -9 + 3\nu^2 - 12 \log \nu + (4 - 12\varsigma) \log^3 \nu, \\ h_2(\varsigma, \nu) &:= 9(9 + 26\nu^2 + \nu^4) \\ &\quad + 8 \log \nu (3 + (-1 + 3\varsigma) \log^2 \nu) (9 - 3\nu^2 + 6 \log \nu + (-2 + 6\varsigma) \log^3 \nu).\end{aligned}$$

The direction belonging to the eigenvalues that can become negative, corresponding to the eigenvalue E_3 of in Lemma 4.12, is

$$\mathbf{a}_1^u(\varsigma, \nu) := \left(1, \frac{1}{12\nu} \left(h_1(\varsigma, \nu) - \sqrt{h_2(\varsigma, \nu)}\right), 1\right).$$

Figure 5b shows the monolayer with a perturbation corresponding to $\mathbf{a}_1^{s_1}$. Here we have chosen the values $d_{u0} = 1$, $d_{uv} = 0.7$, $d_{v0} = 0.3$, $L = 5$ and $\varepsilon = 0.25$. Similarly we get Figure 5c using $\mathbf{a}_1^{s_2}$, and Figure 5a using \mathbf{a}_1^u .

4.4 Discussion and comparison

In Sections 4.2 and 4.3 we found conditions for the stability of monolayers and bilayers with respect to some admissible perturbations. The main results are visualised in Figures 13 and 14 for the monolayer and Figure 15 for the bilayer.

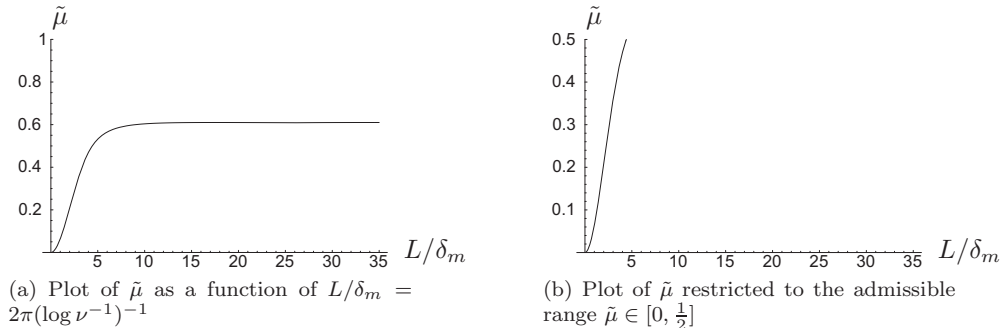


Figure 13: For the plots of $\tilde{\mu}$ from Theorem 4.15 we have approximated $\tilde{\zeta}$ by $\min_{1 \leq j \leq 100} \underline{\zeta}_j$

The monolayer is stable with respect to perturbations of the interface if $\mu \geq \tilde{\mu}$ (Theorem 4.15)₂ and the bilayer is stable with respect to mass-preserving perturbations of the interface if $\zeta \geq \tilde{\zeta}$ (Theorem 4.7).

$\tilde{\mu}$ and $\tilde{\zeta}$ display very similar overall behaviour. They both rapidly increase for small values of L/δ_m or L/δ_b until they settle down around a value for μ or ζ close to 0.6. Around this value both $\tilde{\mu}$ and $\tilde{\zeta}$ oscillate as with increasing L different Fourier modes become dominant. The similarity

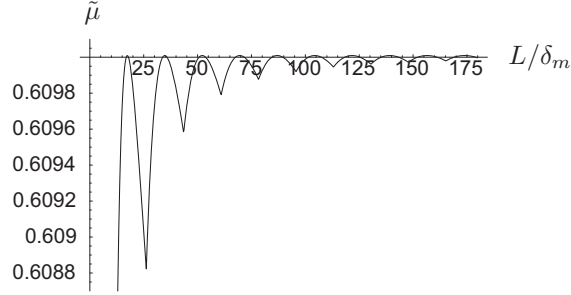


Figure 14: Plot of $\tilde{\mu}$ from Theorem 4.15 as a function of $L/\delta_m = 2\pi(\log \nu^{-1})^{-1}$, showing the small-scale oscillations where different Fourier orders become the dominant contributors.

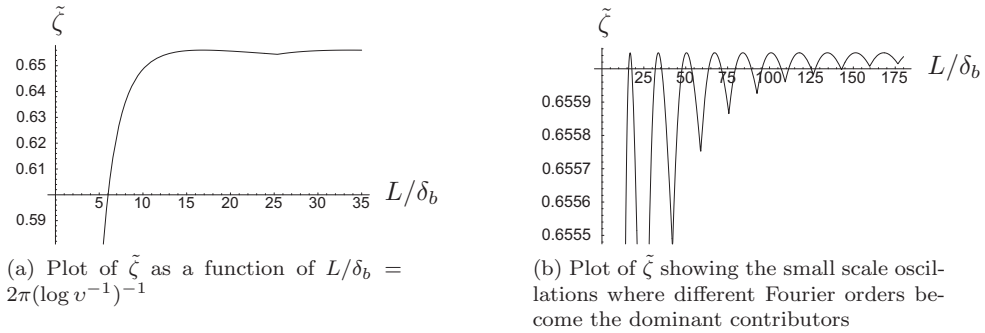


Figure 15: For the plots of $\tilde{\zeta}$ from Theorem 4.7 we have approximated $\tilde{\zeta}$ by $\max_{1 \leq j \leq 100} \zeta_j$

is broken, however, by the restriction of μ to $[0, \frac{1}{2}]$. Because of this the monolayer is unstable for all values of L/δ_m greater than about 6 (see Figure 13b), while the bilayer can be stable for all values of L/δ_b (see Figure 15a).

Remark that higher relative penalisation of the U-V interfaces, i.e. higher values of μ and ζ , improves stability. For the bilayer a sufficiently high value of ζ even guarantees stability in the sense discussed here (Lemma 4.9). This reinforces the notion that d_{uv} plays a special role in the diblock copolymer-homopolymer problem, which was also encountered also in [17, §2.2].

5 Green's function on a periodic two-dimensional strip

When computing the first and second variation of \mathcal{F} for monolayers and bilayers in Section 3 we required an explicit formula for the Green's function of $-\Delta$ on S_L . We present this Green's function here and prove that it satisfies the necessary conditions. For a heuristic derivation we refer to [54, §6.3.1].

Theorem 5.1. *Define $G : S_L \setminus \{(0, 0)\} \rightarrow \mathbb{R}$ in $L^2_{loc}(S_L)$ as follows:*

$$G(x_1, x_2) := \frac{-1}{4\pi} \log \left(2 \cosh \left(\frac{2\pi x_2}{L} \right) - 2 \cos \left(\frac{2\pi x_1}{L} \right) \right). \quad (32)$$

Then the equation $-\Delta G(x_1, x_2) = \delta(x_1, x_2)$ is satisfied with periodic boundary conditions $G(0, x_2) = G(L, x_2)$ and $\frac{\partial}{\partial x_1} G(0, x_2) = \frac{\partial}{\partial x_1} G(L, x_2)$. Writing the Fourier expansion of G in x_1 gives

$$G(x_1, x_2) = -\frac{1}{2L}|x_2| + \frac{1}{2\pi} \sum_{q=1}^{\infty} \frac{1}{q} e^{-2\pi|x_2|q/L} \cos \left(\frac{2\pi x_1 q}{L} \right). \quad (33)$$

Proof. We first prove that G , as given in equation (32), satisfies the equation $-\Delta G(x_1, x_2) = \delta(x_1, x_2)$ in the sense of distributions, i.e. we show that for all $\phi \in C_c^\infty(S_L)$,

$$\int_{S_L} G(x_1, x_2)(-\Delta\phi)(x_1, x_2) dx_1 dx_2 = \phi(0, 0).$$

Note that the constant term $-\frac{1}{4\pi} \log 2$ implicitly present in (32) as the factor 2 in the logarithm is of no importance here and so we will leave it out of subsequent calculations ⁴.

We write

$$\begin{aligned} & \int_{S_L} G(-\Delta\phi) d\mathcal{L}^2 \\ &= \lim_{\varepsilon \rightarrow 0} \int_{S_L \setminus B(0, \varepsilon)} G(-\Delta\phi) d\mathcal{L}^2 \\ &= \lim_{\varepsilon \rightarrow 0} \left(- \int_{\partial B(0, \varepsilon)} G \nabla\phi \cdot \nu d\mathcal{H}^1 - \int_{S_L \setminus B(0, \varepsilon)} \Delta G \phi d\mathcal{L}^2 + \int_{\partial B(0, \varepsilon)} \nabla G \cdot \nu \phi d\mathcal{H}^1 \right), \end{aligned}$$

where $B(0, \varepsilon)$ is the closed ball of radius ε and with the origin as center. ν is the unit outward normal to $S_L \setminus B(0, \varepsilon)$, which means ν points into $B(0, \varepsilon)$. Denote the three terms by $I_\varepsilon, J_\varepsilon$ and K_ε respectively. The integral I_ε vanishes:

$$\begin{aligned} \lim_{\varepsilon \rightarrow 0} |I_\varepsilon| &\leq \lim_{\varepsilon \rightarrow 0} \|\nabla\phi\|_{L^\infty} \int_{\partial B(0, \varepsilon)} |G| d\mathcal{H}^1 \\ &= \lim_{\varepsilon \rightarrow 0} \|\nabla\phi\|_{L^\infty} 2\pi\varepsilon \left| \log\left(\frac{2\pi^2}{L^2}(\varepsilon^2 + \mathcal{O}(\varepsilon^4))\right) \right| = 0. \end{aligned}$$

For J_ε we calculate

$$\nabla G(x_1, x_2) = -\frac{1}{2L} \left[\cosh\left(\frac{2\pi x_2}{L}\right) - \cos\left(\frac{2\pi x_1}{L}\right) \right]^{-1} \begin{pmatrix} \sin\left(\frac{2\pi x_1}{L}\right) \\ \sinh\left(\frac{2\pi x_2}{L}\right) \end{pmatrix}.$$

For notational convenience we will write $C(x_1, x_2) := \cosh\left(\frac{2\pi x_2}{L}\right) - \cos\left(\frac{2\pi x_1}{L}\right)$. Then we can compute that at $(x_1, x_2) \neq (0, 0)$

$$\begin{aligned} \frac{\partial^2}{\partial x_1^2} G(x_1, x_2) &= \frac{\pi}{L^2} \left(C(x_1, x_2)^{-2} \sin^2\left(\frac{2\pi x_1}{L}\right) - C(x_1, x_2)^{-1} \cos\left(\frac{2\pi x_1}{L}\right) \right), \\ \frac{\partial^2}{\partial x_2^2} G(x_1, x_2) &= \frac{\pi}{L^2} \left(C(x_1, x_2)^{-2} \sinh^2\left(\frac{2\pi x_2}{L}\right) - C(x_1, x_2)^{-1} \cosh\left(\frac{2\pi x_2}{L}\right) \right), \end{aligned}$$

which gives $\Delta G(x_1, x_2) = 0$, from which it follows that $J_\varepsilon = 0$ for all $\varepsilon > 0$.

To determine $\lim_{\varepsilon \rightarrow 0} K_\varepsilon$ we approximate G by $G_{\mathbb{R}^2}(x_1, x_2) = -(4\pi)^{-1} \log(x_1^2 + x_2^2)$, the Green's function of $-\Delta$ on \mathbb{R}^2 . Estimating the difference on $\partial B(0, \varepsilon)$ by

$$\begin{aligned} |\nabla G(x_1, x_2) - \nabla G_{\mathbb{R}^2}(x_1, x_2)| &= \left| -\frac{1}{2L} \frac{\frac{2\pi x_1}{L} \vec{e}_1 + \frac{2\pi x_2}{L} \vec{e}_2 + \mathcal{O}((x_1^2 + x_2^2)^{3/2})}{\frac{2\pi^2}{L^2}(x_1^2 + x_2^2) + \mathcal{O}((x_1^2 + x_2^2)^2)} + \frac{1}{2\pi} \frac{x_1 \vec{e}_1 + x_2 \vec{e}_2}{x_1^2 + x_2^2} \right| \\ &= \mathcal{O}((x_1^2 + x_2^2)^{1/2}) \quad \text{as } x_1^2 + x_2^2 = \varepsilon^2 \rightarrow 0, \end{aligned}$$

we calculate

$$\begin{aligned} \lim_{\varepsilon \rightarrow 0} K_\varepsilon &= \lim_{\varepsilon \rightarrow 0} \int_{\partial B(0, \varepsilon)} \nabla(G - G_{\mathbb{R}^2}) \cdot \nu \phi d\mathcal{H}^1 + \lim_{\varepsilon \rightarrow 0} \int_{\partial B(0, \varepsilon)} \nabla G_{\mathbb{R}^2} \cdot \nu \phi d\mathcal{H}^1 \\ &= 0 + \lim_{\varepsilon \rightarrow 0} \frac{1}{2\pi} \int_{\partial B(0, \varepsilon)} \frac{x_1 \vec{e}_1 + x_2 \vec{e}_2}{x_1^2 + x_2^2} \cdot \frac{x_1 \vec{e}_1 + x_2 \vec{e}_2}{(x_1^2 + x_2^2)^{1/2}} \phi(x_1, x_2) d\mathcal{H}^1(x_1, x_2) = \phi(0, 0). \end{aligned}$$

⁴The reason for adding it in (32) in the first place is to get a Fourier series without a term independent of x_1 and x_2 .

Taking these results together shows that $\lim_{\varepsilon \downarrow 0} (I_\varepsilon + J_\varepsilon + K_\varepsilon) = \phi(0, 0)$ and thus $-\Delta G = \delta$ holds in the sense of distributions.

To prove that the Fourier series in (33) corresponds to the Green's function (32), let G be given by (32) and \tilde{G} by (33). Note that for every $x_2 \neq 0$ the series converges absolutely:

$$\sum_{q=1}^{\infty} \left| \frac{1}{q} e^{-\frac{2\pi|x_2|q}{L}} \cos\left(\frac{2\pi x_1 q}{L}\right) \right| \leq \sum_{q=1}^{\infty} \left(e^{-\frac{2\pi|x_2|}{L}} \right)^q = \frac{e^{-\frac{2\pi|x_2|}{L}}}{1 - e^{-\frac{2\pi|x_2|}{L}}}.$$

If $x_2 \neq 0$ we then calculate

$$\begin{aligned} \sum_{q=1}^{\infty} \frac{1}{q} e^{-\frac{2\pi|x_2|q}{L}} \cos\left(\frac{2\pi q x_1}{L}\right) &= \operatorname{Re} \sum_{q=1}^{\infty} \frac{1}{q} e^{\frac{2\pi}{L}(-|x_2| + i x_1)} \\ &= -\operatorname{Re} \log\left(1 - e^{\frac{2\pi}{L}(-|x_2| + i x_1)}\right) \\ &= -\log\left|1 - e^{\frac{2\pi}{L}(-|x_2| + i x_1)}\right| \\ &= -\frac{1}{2} \log\left(1 - 2e^{-\frac{2\pi|x_2|}{L}} \cos\left(\frac{2\pi x_1}{L}\right) + e^{-\frac{4\pi|x_2|}{L}}\right) \\ &= -\frac{1}{2} \log\left(2e^{-\frac{2\pi|x_2|}{L}} \left(\frac{1}{2} e^{\frac{2\pi|x_2|}{L}} - \cos\left(\frac{2\pi x_1}{L}\right) + \frac{1}{2} e^{-\frac{2\pi|x_2|}{L}}\right)\right) \\ &= \frac{\pi}{L}|x_2| - \frac{1}{2} \log\left(2 \cosh\left(\frac{2\pi|x_2|}{L}\right) - 2 \cos\left(\frac{2\pi x_1}{L}\right)\right), \end{aligned} \quad (34)$$

so that the partial sums $\sum_{q=1}^{\ell} \frac{1}{q} e^{-\frac{2\pi|x_2|q}{L}} \cos\left(\frac{2\pi q x_1}{L}\right)$ converge pointwise to $2\pi G(x_1, x_2) + \frac{\pi}{L}|x_2|$ for almost all $(x_1, x_2) \in S_L$. Since the partial sums are all bounded by the L^2_{loc} -function on the right hand side of (34) the Dominated Convergence Theorem yields $\tilde{G} \in L^2(S_L)$. Together with $G = \tilde{G}$ a.e. on S_L this shows that $G = \tilde{G}$ in $L^2_{\text{loc}}(S_L)$. \square

Corollary 5.2. *Let G be as in (33) and let $x_2 \in \mathbb{R} \setminus \{0\}$. Then*

$$\int_0^L G(x_1, x_2) dx_1 = -\frac{1}{2}|x_2|.$$

Proof. For all $q \geq 1$,

$$\int_0^L \cos\left(\frac{2\pi q x_1}{L}\right) dx_1 = 0.$$

\square

Also note that $G(-x_1, x_2) = G(x_1, x_2)$ and $G(x_1, -x_2) = G(x_1, x_2)$.

6 Discussion and conclusions

6.1 Comparing mono- and bilayers

In this paper we showed that bilayers can be both stable and unstable, depending on the parameters: when the U-V interface penalty is strong enough relative to the penalties of the other interfaces, the bilayer is stable. On the other hand, monolayers are unstable as soon as the strip is wide enough to accommodate the unstable wavelengths, regardless of the values of the interface penalisation.

The bilayer can be thought of as two juxtaposed monolayers, and therefore the question presents itself how the unstable mode of the monolayer is prevented in the bilayer context. The correct answer seems to be that the unstable mode is actually not prevented at all; it continues to exist in the context of the bilayer, as can be witnessed in Figures 5a and (especially) 7b.

The reason why this unstable mode does not make every bilayer unstable lies in the admissible values of the coefficients, which are different in the two cases. For the VUV bilayer, for instance, the value of the U-0 interface penalty d_{u0} is irrelevant; therefore, by choosing $d_{u0} := d_{v0} + d_{uv}$, every choice of d_{uv} and d_{v0} becomes admissible, and most importantly, the case of purely U-V penalisation ($\zeta \approx 1$, or $d_{v0} \approx 0$) is therefore allowed. For the monolayer, however, the conditions (3) imply that the two side interfaces (0-U and V-0) are necessarily penalised at least half as strongly as the central (U-V) interface. Most of the white (stable) region in Figure 12b therefore is inaccessible, and only the unstable region remains as can be seen in Figure 12a (Figures 12 only show stability of the first Fourier mode, but the situation is similar for the higher modes).

6.2 Comparison with [34]

In previous work [34] one of the authors (Peletier) and Röger studied a related functional,

$$\mathcal{G}_\varepsilon(u, v) := \begin{cases} \varepsilon \int_{\mathbb{R}^2} |\nabla u| + \frac{1}{\varepsilon} d_1(u, v) & \text{if } (u, v) \in \mathcal{K}_\varepsilon, \\ \infty & \text{otherwise.} \end{cases} \quad (35)$$

Here $d_1(\cdot, \cdot)$ is the Monge-Kantorovich distance with cost function $c(x, y) = |x - y|$, [56], and

$$\mathcal{K}_\varepsilon := \left\{ (u, v) \in \text{BV}(\mathbb{R}^2; \{0, 1/\varepsilon\}) \times L^1(\mathbb{R}^2; \{0, 1/\varepsilon\}) : uv = 0 \text{ a.e., and } \int_{\mathbb{R}^2} u = \int_{\mathbb{R}^2} v = M \right\}.$$

Apart from the choices $c_0 = c_v = 0$ and $c_u = 1$, the main difference between \mathcal{F} and (35) is the different non-local term.

The scaling (constant mass but increasing amplitude $1/\varepsilon$) implies that the supports of u and v shrink to zero measure. The main goal in [34] was to investigate the limit $\varepsilon \rightarrow 0$ and characterise the limiting structures and their energy.

The main result, a Γ -convergence theorem, can be interpreted as stating—in a very weak sense—that the limiting structures are VUV bilayers; in the limit $\varepsilon \rightarrow 0$ these bilayers have a thickness equal to 4ε and their curvature is bounded in L^2 . Most importantly, in connection with the present paper, the limit energy depends on the curvature in a stable way: the energy is minimal for straight bilayers and increases with curvature.

This result compares well with the results of this paper. The functional \mathcal{G}_ε of [34] penalises only U-V and U-0 interfaces; the V-0 interface is free, or in terms of this paper $\zeta = 1$. Both in [34] and in the present paper we therefore find that bilayers of optimal width are stable, although the precise results and their methods of proof are very different.

6.3 Comparison with ‘wriggled lamellar’ solutions

In a series of papers [30, 37, 40] Muratov and Ren & Wei investigate the stability of one-dimensional layered (lamellar) structures for copolymer melts—the case $u + v \equiv 1$. They find that for a critical value of the lamellar spacing the straight lamellar structures become unstable and a stable branch of curved, ‘wriggled’ lamellar structures bifurcates. Muratov considers unbounded domains and finds that the loss of stability happens at *exactly* the optimal value of the width: for any larger value of the width unstable directions exist with very large wavelength. Ren and Wei consider bounded domains, which provides a natural limit on the wavelength of perturbations, and consequently they find that at the optimal width the straight lamellar structures are stable, and the bifurcation occurs at slightly larger width.

The system studied in this paper is different in that there are three types of interfaces, not one; for comparison purposes one can identify the pure-melt case described above with the case of pure U-V interface penalisation for bilayers ($\zeta = 1$). In this case the bilayer of optimal width is stable, and this result mirrors the stability result of Ren and Wei for optimal-width lamellar structures.

6.4 Generalizations and extensions

One might wonder whether the functional \mathcal{F} depends in a smooth manner on the perturbations. The calculation of the second derivative of the functional in the melt case done by Choksi and Sternberg [10] suggests that the second derivative of \mathcal{F} depends continuously on $W^{1,2}$ -regular perturbations of the interfaces. In that case the functional \mathcal{F} is of class C^2 , and the linear stability analysis of the current paper automatically implies the equivalent nonlinear stability properties.

One can also wonder whether the class of perturbations that are considered—those described by functions of the variable $x_1 \in \mathbb{T}_L$ —is not too restrictive. The class of all perturbations that are small in L^1 , for instance, also includes many perturbations with small inclusions of one phase in another, which are not covered here. We believe that these will generally be less advantageous, since the results of this chapter show that perturbations with fast oscillations are energetically expensive (because the layers are stable with respect to the admissible perturbations for most values of the surface tension coefficients if L is small). The same conclusion can be reached by a slightly different, heuristic argument as follows. Within the class of uniformly bounded functions the H^{-1} -norm is continuous with respect to the L^1 -topology, as can be seen from

$$\|f\|_{H^{-1}}^2 = \int f\varphi \leq \|f\|_{L^2}\|\varphi\|_{L^2} \leq C\|f\|_{L^2}^2 \leq C\|f\|_{L^1}\|f\|_{L^\infty},$$

where φ solves $-\Delta\varphi = f$. Therefore within that class of functions the H^{-1} -norm is also continuous with respect to the area of the inclusion; for small inclusions, with a large circumference-to-area ratio, a possible decrease in the H^{-1} -norm is thus dwarfed by the increase in interfacial length associated with such an inclusion.

Note that the problem has not completely been non-dimensionalised; it is possible to rescale the problem by the length scale L , resulting in a three-parameter problem (in the rescaled parameters c_0 , c_u , and c_v). Instead we keep the length scale explicitly in the problem to illustrate the length-scale dependence of the stability properties.

6.5 Diffuse interface model

The functional \mathcal{F} is the sharp interface limit (via Γ -convergence) of a well-known diffuse-interface functional [28, 6]

$$\mathcal{F}_\varepsilon(u, v) = \int \left[\frac{\varepsilon}{2} |\nabla u|^2 + \frac{\varepsilon}{2} |\nabla v|^2 + \frac{\varepsilon}{2} |\nabla(u+v)|^2 + \varepsilon^{-1} W(u, v) \right] dx + \frac{1}{2} \|u - v\|_{H^{-1}}^2.$$

Here W is a triple-well potential with wells at $(0, 0)$, $(1, 0)$, and $(0, 1)$. The coefficients d_{uv} , d_{u0} , and d_{v0} in the sharp interface limit depend on the specific form of W via

$$d_{kl} := 2 \inf \left\{ \int_0^1 \sqrt{W(\gamma(t))} |\gamma'(t)| dt : \gamma \in C^1([0, 1]; (\mathbb{R}_+)^n), \gamma(0) = \alpha_k, \gamma(1) = \alpha_l \right\},$$

where $\alpha_u = (1, 0)$, $\alpha_v = (0, 1)$, and $\alpha_0 = (0, 0)$.

By the properties of Γ -convergence minimisers of \mathcal{F}_ε converge to minimisers of \mathcal{F} [12, Corollary 7.17]. Therefore our results indicate that in the regions of their respective instability monolayers and bilayers are not minimisers for \mathcal{F}_ε for small ε .

A Relevance of energy per unit mass for partial localisation

Throughout this paper we concentrate on layered structures with a specific width: the width that minimises the ratio of (one-dimensional) energy to (one-dimensional) mass. The origin for this choice lies in our interest in partially localised structures, as we now explain.

Since we are interested in long thin structures, we might first ask ourself the question what minimisers of \mathcal{F} on the full domain \mathbb{R}^2 look like if we restrict the admissible functions to be rectangles with a fixed mass, oriented such that the long axis is parallel to the x_1 -axis.

If the rectangle has a large aspect ratio, the structure is roughly constant in the x_1 -direction. We can interpret the rectangle then as a one-dimensional structure in the x_2 -direction, extended trivially in the x_1 -direction and cut off at a certain length, a . In [17] it is proven that for such a trivially extended one-dimensional structure the energy \mathcal{F} per mass M is approximately equal to the one-dimensional energy F_{1D} per mass of the cross-section M_{1D} :

$$\frac{\mathcal{F}}{M} = \frac{F_{1D}}{M_{1D}} + \mathcal{O}(1/a), \text{ for } a \rightarrow \infty.$$

Put differently: although the energy depends on the structure in a nonlocal manner, for large mass (i.e. long rectangles) the energy is essentially equal to the one-dimensional energy of the cross-section times the length of the rectangle. Effects near the cut off points are less important.

This implies that the minimiser of \mathcal{F} in the class of rectangles with large constrained mass should have a thickness M_{1D} such that F_{1D}/M_{1D} is minimal. Also when studying the stability of layered structures, it thus makes sense to concentrate on structures of optimal width, in the sense as described above.

In a monolayer of optimal width the U- and V-layers both have width [17]

$$\delta_m := \left(\frac{3}{2}\right)^{1/3} (c_0 + c_u + c_v)^{1/3},$$

while for the bilayer the thickness of the inner layer is

$$2\delta_b := 6^{1/3}(c_0 + c_u + 2c_v)^{1/3} \text{ (VUV)} \quad \text{or} \quad 2\delta_b := 6^{1/3}(c_0 + 2c_u + c_v)^{1/3} \text{ (UVU)}.$$

B Relevance of the choice $c_u = c_v$ for monolayers

The choice $c_u = c_v$ for monolayers is similarly inspired by our interest in partial localisation and more or less forced upon us by the periodicity in the x_1 -direction. If the U-0 and V-0 interfaces are penalised unequally, then a monolayer structure in \mathbb{R}^2 likely will tend to curve, in order to reduce the length of the ‘expensive’ interface at the expense of the ‘cheap’ interface.

When $c_u \neq c_v$, therefore, a straight monolayer is not even stationary under perturbations that allow for curving of the whole monolayer. The setup in the context of the strip S_L disallows such curving over the whole length of the layer because of the periodicity in the x_1 -direction. Therefore this instationarity is rendered invisible on S_L . However, with our interest in partial localisation in mind we make the choice $c_u = c_v$ in the case of monolayers throughout this paper.

C Proof of Theorem 3.6

For the interfacial terms we directly compute from (10)

$$\begin{aligned} \frac{d^2}{d\varepsilon^2} \left(c_0 \int_{S_L} |\nabla(u_\varepsilon + v_\varepsilon)| + c_u \int_{S_L} |\nabla u_\varepsilon| + c_v \int_{S_L} |\nabla v_\varepsilon| \right) \Big|_{\varepsilon=0} = \\ \int_0^L \left(d_{uv} [p_1'^2 + p_3'^2] + d_{v0} [p_2'^2 + p_4'^2] \right) dx. \end{aligned} \quad (36)$$

In order to compute $\frac{d^2}{d\varepsilon^2} \|u_\varepsilon - v_\varepsilon\|_{H^{-1}(S_L)}^2 \Big|_{\varepsilon=0}$ we split up the norm as follows:

$$\|u_\varepsilon - v_\varepsilon\|_{H^{-1}(S_L)}^2 = \int_0^L \int_0^L f_\varepsilon(x_1, \xi_1) d\xi_1 dx_1, \quad (37)$$

where

$$\begin{aligned}
f_\varepsilon(x_1, \xi_1) := & \int_{-2\delta_b - \varepsilon p_4(x_1)}^{-\delta_b - \varepsilon p_3(x_1)} \int_{-2\delta_b - \varepsilon p_4(\xi_1)}^{-\delta_b - \varepsilon p_3(\xi_1)} G(x - \xi) d\xi_2 dx_2 + \int_{-\delta_b - \varepsilon p_3(x_1)}^{\delta_b + \varepsilon p_1(x_1)} \int_{-\delta_b - \varepsilon p_3(\xi_1)}^{\delta_b + \varepsilon p_1(\xi_1)} G(x - \xi) d\xi_2 dx_2 \\
& + \int_{\delta_b + \varepsilon p_1(x_1)}^{2\delta_b + \varepsilon p_2(x_1)} \int_{\delta_b + \varepsilon p_1(\xi_1)}^{2\delta_b + \varepsilon p_2(\xi_1)} G(x - \xi) d\xi_2 dx_2 \\
& - 2 \int_{-\delta_b - \varepsilon p_3(x_1)}^{\delta_b + \varepsilon p_1(x_1)} \int_{-2\delta_b - \varepsilon p_4(\xi_1)}^{-\delta_b - \varepsilon p_3(\xi_1)} G(x - \xi) d\xi_2 dx_2 - 2 \int_{\delta_b + \varepsilon p_1(x_1)}^{2\delta_b + \varepsilon p_2(x_1)} \int_{-\delta_b - \varepsilon p_3(\xi_1)}^{\delta_b + \varepsilon p_1(\xi_1)} G(x - \xi) d\xi_2 dx_2 \\
& + 2 \int_{\delta_b + \varepsilon p_1(x_1)}^{2\delta_b + \varepsilon p_2(x_1)} \int_{-2\delta_b - \varepsilon p_4(\xi_1)}^{-\delta_b - \varepsilon p_3(\xi_1)} G(x - \xi) d\xi_2 dx_2 \tag{38}
\end{aligned}$$

We compute now one of these terms in its general form. Let $n_1, n_2, n_3, n_4 \in \{-2, -1, 1, 2\}$, $r_1, r_2 \in \{p_1(x_1), p_2(x_1), -p_3(x_1), -p_4(x_1)\}$ and $r_3, r_4 \in \{p_1(\xi_1), p_2(\xi_1), -p_3(\xi_1), -p_4(\xi_1)\}$ (with $n_1 < n_2 < n_3 < n_4$ and $r_1 < r_2 < r_3 < r_4$), then we want to compute

$$I = \frac{d^2}{d\varepsilon^2} \int_{n_1\delta_b + \varepsilon r_1}^{n_2\delta_b + \varepsilon r_2} \int_{n_3\delta_b + \varepsilon r_3}^{n_4\delta_b + \varepsilon r_4} G(\cdot, x_2 - \xi_2) d\xi_2 dx_2 \Big|_{\varepsilon=0}.$$

We can split up the integral over $[n_1\delta_b + \varepsilon r_1, n_2\delta_b + \varepsilon r_2] \times [n_3\delta_b + \varepsilon r_3, n_4\delta_b + \varepsilon r_4]$ into nine integrals over the domains

$$\begin{aligned}
& [n_2\delta_b, n_2\delta_b + \varepsilon r_2] \times [n_3\delta_b + \varepsilon r_3, n_3\delta_b], & [n_2\delta_b, n_2\delta_b + \varepsilon r_2] \times [n_3\delta_b, n_4\delta_b], \\
& [n_2\delta_b, n_2\delta_b + \varepsilon r_2] \times [n_4\delta_b, n_4\delta_b + \varepsilon r_4], & [n_1\delta_b, n_2\delta_b] \times [n_3\delta_b + \varepsilon r_3, n_3\delta_b], \\
& [n_1\delta_b, n_2\delta_b] \times [n_3\delta_b, n_4\delta_b], & [n_1\delta_b, n_2\delta_b] \times [n_4\delta_b, n_4\delta_b + \varepsilon r_4], \\
& [n_1\delta_b + \varepsilon r_1, n_1\delta_b] \times [n_3\delta_b + \varepsilon r_3, n_3\delta_b], & [n_1\delta_b + \varepsilon r_1, n_1\delta_b] \times [n_3\delta_b, n_4\delta_b], \\
& [n_1\delta_b + \varepsilon r_1, n_1\delta_b] \times [n_4\delta_b, n_4\delta_b + \varepsilon r_4].
\end{aligned}$$

We compute two of these integrals. The others are computed in a similar vein. $G_{,2}$ denotes the partial derivative of G with respect to its second argument.

$$\begin{aligned}
& \frac{d^2}{d\varepsilon^2} \int_{n_2\delta_b}^{n_2\delta_b + \varepsilon r_2} \int_{n_3\delta_b + \varepsilon r_3}^{n_3\delta_b} G(\cdot, x_2 - \xi_2) d\xi_2 dx_2 \Big|_{\varepsilon=0} \\
& = \frac{d^2}{d\varepsilon^2} \int_0^{r_2} \int_{r_3}^0 \varepsilon^2 G(\cdot, \varepsilon(\tilde{x}_2 - \tilde{\xi}_2) + (n_2 - n_3)\delta_b) d\tilde{\xi}_2 d\tilde{x}_2 \Big|_{\varepsilon=0} \\
& = \frac{d}{d\varepsilon} \int_0^{r_2} \int_{r_3}^0 \left[2\varepsilon G(\cdot, \varepsilon(\tilde{x}_2 - \tilde{\xi}_2) + (n_2 - n_3)\delta_b) + \varepsilon^2(\tilde{x}_2 - \tilde{\xi}_2) G_{,2}(\cdot, \varepsilon(\tilde{x}_2 - \tilde{\xi}_2) + (n_2 - n_3)\delta_b) \right] d\tilde{\xi}_2 d\tilde{x}_2 \Big|_{\varepsilon=0} \\
& = 2 \int_0^{r_2} \int_{r_3}^0 G(\cdot, (n_2 - n_3)\delta_b) d\tilde{\xi}_2 d\tilde{x}_2 \\
& = -2r_2 r_3 G(\cdot, (n_2 - n_3)\delta_b).
\end{aligned}$$

Another kind of integral we encounter is

$$\begin{aligned}
& \left. \frac{d^2}{d\varepsilon^2} \int_{n_2\delta_b}^{n_2\delta_b+\varepsilon r_2} \int_{n_3\delta_b}^{n_4\delta_b} G(\cdot, x_2 - \xi_2) d\xi_2 dx_2 \right|_{\varepsilon=0} \\
&= - \left. \frac{d^2}{d\varepsilon^2} \int_0^{r_2} \int_{(n_2-n_3)\delta_b}^{(n_2-n_4)\delta_b} \varepsilon G(\cdot, \varepsilon\tilde{x}_2 + \tilde{\xi}_2) d\tilde{\xi}_2 d\tilde{x}_2 \right|_{\varepsilon=0} \\
&= - \left. \frac{d}{d\varepsilon} \int_0^{r_2} \int_{(n_2-n_3)\delta_b}^{(n_2-n_4)\delta_b} \left[G(\cdot, \varepsilon\tilde{x}_2 + \tilde{\xi}_2) + \varepsilon\tilde{x}_2 G_{,2}(\cdot, \varepsilon\tilde{x}_2 + \tilde{\xi}_2) \right] d\tilde{\xi}_2 d\tilde{x}_2 \right|_{\varepsilon=0} \\
&= - \int_0^{r_2} \int_{(n_2-n_3)\delta_b}^{(n_2-n_4)\delta_b} 2\tilde{x}_2 G_{,2}(\cdot, \tilde{\xi}_2) d\tilde{\xi}_2 d\tilde{x}_2 \\
&= r_2^2 \left(G((n_2-n_3)\delta_b) - G((n_2-n_4)\delta_b) \right).
\end{aligned}$$

Combining all integrals we find

$$\begin{aligned}
I &= -2r_2r_3G(\cdot, (n_2-n_3)\delta_b) + r_2^2 \left(G(\cdot, (n_2-n_3)\delta_b) - G(\cdot, (n_2-n_4)\delta_b) \right) + 2r_2r_4G(\cdot, (n_2-n_4)\delta_b) \\
&\quad + r_3^2 \left(G(\cdot, (n_2-n_3)\delta_b) - G(\cdot, (n_1-n_3)\delta_b) \right) - r_4^2 \left(G(\cdot, (n_2-n_4)\delta_b) - G(\cdot, (n_1-n_4)\delta_b) \right) \\
&\quad + 2r_1r_3G(\cdot, (n_1-n_3)\delta_b) + r_1^2 \left(G(\cdot, (n_1-n_4)\delta_b) - G(\cdot, (n_1-n_3)\delta_b) \right) - 2r_1r_4G(\cdot, (n_1-n_4)\delta_b).
\end{aligned}$$

Applying this result to (38) while keeping in mind that $G(-x_1, \cdot) = G(x_1, \cdot)$ and $G(\cdot, -x_2) = G(\cdot, x_2)$, we find

$$\begin{aligned}
f_\varepsilon(x_1, \xi_1) &= \left[-8p_1^2(x_1) + 8p_1(x_1)p_1(\xi_1) - 2p_2^2(x_1) + 2p_2(x_1)p_2(\xi_1) \right. \\
&\quad \left. - 8p_3^2(x_1) + 8p_3(x_1)p_3(\xi_1) - 2p_4^2(x_1) + 2p_4(x_1)p_4(\xi_1) \right] G(x_1 - \xi_1, 0) \\
&\quad + \left[4p_1(x_1) - 8p_1(x_1)p_2(\xi_1) + 4p_2^2(x_1) + 4p_3^2(x_1) - 8p_3(x_1)p_4(\xi_1) + 4p_4^2(x_1) \right] G(x_1 - \xi_1, \delta_b) \\
&\quad + \left[8p_1^2(x_1) + 16p_1(x_1)p_3(\xi_1) + 8p_3^2(x_1) \right] G(x_1 - \xi_1, 2\delta_b) \\
&\quad - \left[4p_1^2(x_1) + 4p_2^2(x_1) + 8p_2(x_1)p_3(\xi_1) + 4p_3^2(x_1) + 8p_1(x_1)p_4(\xi_1) + 4p_4^2(\xi_1) \right] G(x_1 - \xi_1, 3\delta_b) \\
&\quad + \left[2p_2^2(x_1) + 4p_2(x_1)p_4(\xi_1) + 2p_4^2(x_1) \right] G(x_1 - \xi_1, 4\delta_b),
\end{aligned}$$

where we have used that in (37) the integrations over x_1 and ξ_1 are indistinguishable.

Note that, by Corollary 5.2, for $\xi \in \mathbb{T}_L, r \in \mathbb{R}$

$$\int_0^L G(x - \xi, r) dx = \int_0^L G(x, r) dx = -\frac{1}{2}|r|.$$

Using this, as well as equations (4-5) and the equality $\overline{\hat{G}(q, r)} = \hat{G}(q, r)$ for $r \in \mathbb{R}$, we find

$$\begin{aligned}
\left. \frac{d^2}{d\varepsilon^2} \|u_\varepsilon - v_\varepsilon\|_{H^{-1}(S_L)}^2 \right|_{\varepsilon=0} &= -4\delta_b \sum_{q \in \mathbb{Z}} (|\hat{p}_1(q)|^2 + |\hat{p}_3(q)|^2) \\
&\quad + L^{\frac{1}{2}} \sum_{q \in \mathbb{Z}} \left[\{8|\hat{p}_1(q)|^2 + 2|\hat{p}_2(q)|^2 + 8|\hat{p}_3(q)|^2 + 2|\hat{p}_4(q)|^2\} \hat{G}(q, 0) \right. \\
&\quad \quad - 8\{\hat{p}_1(q)\overline{\hat{p}_2(q)} + \hat{p}_3(q)\overline{\hat{p}_4(q)}\} \hat{G}(q, \delta_b) \\
&\quad \quad + 16\hat{p}_1(q)\overline{\hat{p}_3(q)} \hat{G}(q, 2\delta_b) \\
&\quad \quad - 8\{\hat{p}_2(q)\overline{\hat{p}_3(q)} + \hat{p}_1(q)\overline{\hat{p}_4(q)}\} \hat{G}(q, 3\delta_b) \\
&\quad \quad \left. + 4\hat{p}_2(q)\overline{\hat{p}_4(q)} \hat{G}(q, 4\delta_b) \right]. \tag{39}
\end{aligned}$$

Adding the results (36) and (39), we get

$$\begin{aligned}
\left. \frac{d^2}{d\varepsilon^2} \mathcal{F}(u_\varepsilon, v_\varepsilon) \right|_{\varepsilon=0} &= \int_0^L \left(d_{uv} [p_1'^2 + p_3'^2] + d_{v0} [p_2'^2 + p_4'^2] \right) dx \\
&+ L^{\frac{1}{2}} \sum_{q \in \mathbb{Z}} \left[\{ 8|\hat{p}_1(q)|^2 + 2|\hat{p}_2(q)|^2 + 8|\hat{p}_3(q)|^2 + 2|\hat{p}_4(q)|^2 \} \hat{G}(q, 0) \right. \\
&\quad - 8\{ \hat{p}_1(q)\overline{\hat{p}_2(q)} + \hat{p}_3(q)\overline{\hat{p}_4(q)} \} \hat{G}(q, \delta_b) \\
&\quad + 16\hat{p}_1(q)\overline{\hat{p}_3(q)} \hat{G}(q, 2\delta_b) \\
&\quad - 8\{ \hat{p}_2(q)\overline{\hat{p}_3(q)} + \hat{p}_1(q)\overline{\hat{p}_4(q)} \} \hat{G}(q, 3\delta_b) \\
&\quad \left. + 4\hat{p}_2(q)\overline{\hat{p}_4(q)} \hat{G}(q, 4\delta_b) \right] \\
&- 4\delta_b \sum_{q \in \mathbb{Z}} (|\hat{p}_1(q)|^2 + |\hat{p}_3(q)|^2).
\end{aligned}$$

Because we have, for all $q, \tilde{q} \in \mathbb{N}$,

$$\begin{aligned}
\frac{2}{L} \int_0^L \sin\left(\frac{2\pi x q}{L}\right) \sin\left(\frac{2\pi x \tilde{q}}{L}\right) dx &= \frac{2}{L} \int_0^L \cos\left(\frac{2\pi x q}{L}\right) \cos\left(\frac{2\pi x \tilde{q}}{L}\right) dx = \delta_{q\tilde{q}}, \\
\frac{2}{L} \int_0^L \sin\left(\frac{2\pi x q}{L}\right) \cos\left(\frac{2\pi x \tilde{q}}{L}\right) dx &= 0,
\end{aligned}$$

the integral over the derivatives in the second variation gives us

$$\begin{aligned}
&\sum_{j=1}^{\infty} \left(\frac{2\pi j}{L}\right)^2 \left[d_{uv} \{ (a_{1,j})^2 + (a_{3,j})^2 + (b_{1,j})^2 + (b_{3,j})^2 \} \right. \\
&\quad \left. + d_{v0} \{ (a_{2,j})^2 + (a_{4,j})^2 + (b_{2,j})^2 + (b_{4,j})^2 \} \right].
\end{aligned}$$

Because p is \mathbb{R}^4 -valued, $\overline{\hat{p}(q)} = \hat{p}(-q)$. Furthermore $\hat{G}(-q, x_2) = \hat{G}(q, x_2)$ by equation (32). This enables us to write terms as follows, for $k, l \in \{1, 2, 3, 4\}$:

$$\sum_{q \in \mathbb{Z}} \hat{p}_k(q) \overline{\hat{p}_l(q)} \hat{G}(q, x_2) = \hat{p}_k(0) \hat{p}_l(0) \hat{G}(0, x_2) + 2\text{Re} \sum_{q=1}^{\infty} \hat{p}_k(q) \overline{\hat{p}_l(q)} \hat{G}(q, x_2).$$

Note that, for $k \in \{1, 2, 3, 4\}$, $q \in \mathbb{Z} \setminus \{0\}$, we have $\hat{p}_k(q) = \frac{1}{\sqrt{2}} \left(a_q^{(k)} - i b_q^{(k)} \right)$ and $\overline{\hat{p}_k(q)} = \frac{1}{\sqrt{2}} \left(a_q^{(k)} + i b_q^{(k)} \right)$ and thus, for $l \in \{1, 2, 3, 4\}$,

$$\text{Re} \hat{p}_k(q) \overline{\hat{p}_l(q)} = \frac{1}{2} \left(a_q^{(k)} a_q^{(l)} + b_q^{(k)} b_q^{(l)} \right).$$

From the Fourier series (33) we get furthermore that

$$\begin{aligned}
\hat{G}(0, x_2) &= -\frac{1}{2\sqrt{L}} |x_2|, \\
\hat{G}(q, x_2) &= \frac{\sqrt{L}}{4\pi q} e^{-2\pi |x_2| q/L}, \text{ for } q \geq 1.
\end{aligned}$$

Using these results in the expression for the second variation yields the desired result.

D Detailed calculations in the proof of Lemma 4.5

In this appendix we prove (22). Since $0 < v < 1$ we have $3(-1 + v^4) - 4(-1 + \zeta) \log^3 v < 0$ and thus $G_- < 0 \iff h_- > 0$. Because $\frac{4}{3} \log^6 v$, the coefficient in front of ζ^2 in h_- , is positive, we

know that h_- is positive for $\zeta \in [0, \zeta_1(v)) \cup (\zeta_2(v), 1]$, where $\zeta_{1,2}$ are the v -dependent zeros of h_- , with $\zeta_1 \leq \zeta_2$. These zeroes are given by

$$\begin{aligned} \zeta_{1,2}(v) = (8 \log^3 v)^{-1} & \left(9 - 12v^2 + 3v^4 + (4 \log v)(3 + \log^2 v) \right. \\ & \pm \left\{ 225 - 504v^2 + 342v^4 - 72v^6 + 9v^8 + (360 - 288v^2 - 72v^4) \log v \right. \\ & \left. \left. + 144 \log^2 v + (-120 + 96v^2 + 24v^4) \log^3 v - 96 \log^4 v + 16 \log^6 v \right\}^{\frac{1}{2}} \right). \end{aligned}$$

We take the plus sign in ζ_1 and the minus sign in ζ_2 . In this way the negativity of $(8 \log^3 v)^{-1}$ ensures that $\zeta_1 \leq \zeta_2$. Plots of ζ_1 and ζ_2 are given in Figure 16.

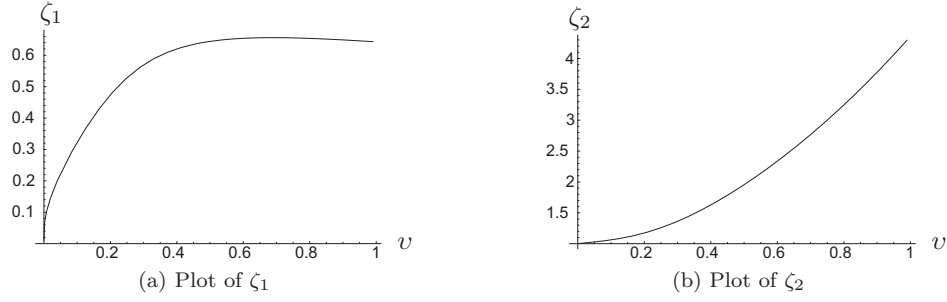


Figure 16:

We start by proving that $9 - 12v^2 + 3v^4 + (4 \log v)(3 + \log^2 v) < 0$ on $(0, 1)$. The equation

$$v \frac{d}{dv} (2v^4 - 2v^2 + \log v) = 8v^4 - 4v^2 + 1 = 0$$

has no real solutions on $(0, 1)$ and so $\frac{1}{2}v \frac{d}{dv} (v^4 - 2v^2 + \log^2 v + 1) = 2v^4 - 2v^2 + \log v \leq 0$ on $(0, 1]$, with equality iff $v = 1$. This in turn shows that $12v \frac{d}{dv} (9 - 12v^2 + 3v^4 + (4 \log v)(3 + \log^2 v)) = v^4 - 2v^2 + \log^2 v + 1 \geq 0$ on $(0, 1]$, with equality iff $v = 1$, from which $9 - 12v^2 + 3v^4 + (4 \log v)(3 + \log^2 v) < 0$ follows. Consequently, since $(8 \log^3 v)^{-1} < 0$, we have that $\zeta_2 > 0$.

Next we calculate

$$\frac{d}{dv} \left(3 \log v - 3 + \frac{6}{v^2 + 1} - \log^3 v \right) = \frac{3}{v} - \frac{12v}{(v^2 + 1)^2} - \frac{3}{v} \log^2 v.$$

This is equal to zero if and only if $\log^2 v = \frac{(1-v^2)^2}{(1+v^2)^2}$, which leads to $v = e^{-\frac{1-v^2}{1+v^2}}$. We will now prove

$$v \in [0, 1] \wedge v = e^{-\frac{1-v^2}{1+v^2}} \iff v = 1.$$

Since $v = 1$ clearly satisfies the equation on the left, it remains to show that there are not more solutions. We start by computing

$$\begin{aligned} \frac{d}{dv} \left(e^{-\frac{1-v^2}{1+v^2}} - v \right) &= \frac{4v}{(1+v^2)^2} e^{-\frac{1-v^2}{1+v^2}} - 1; \\ \frac{d^2}{dv^2} \left(e^{-\frac{1-v^2}{1+v^2}} - v \right) &= \frac{1}{(1+v^2)^4} (-12v^4 + 8v^2 + 4) e^{-\frac{1-v^2}{1+v^2}}. \end{aligned}$$

On $[0, 1]$ we have

$$\frac{d^2}{dv^2} \left(e^{-\frac{1-v^2}{1+v^2}} - v \right) = 0 \iff -12v^4 + 8v^2 + 4 = 0 \iff v = 1,$$

showing that $\frac{d}{dv} \left(e^{\frac{-1+v^2}{1+v^2}} - v \right)$ has at most one zero on $[0, 1]$ and thus its only zero is at $v = 1$, which in turn shows that also $e^{\frac{-1+v^2}{1+v^2}} - v$ has at most one zero on $[0, 1]$, which is what we set out to prove. This now leads us to conclude

$$\frac{d}{dv} \left(3 \log v - 3 + \frac{6}{v^2 + 1} - \log^3 v \right) = 0 \iff v = 1.$$

This means that $3 \log v - 3 + \frac{6}{v^2 + 1} - \log^3 v$ has a minimum at $v = 1$ and thus this expression is positive on $(0, 1)$. Then

$$\begin{aligned} & \left\{ (9 - 12v^2 + 3v^4 + (4 \log v)(3 + \log^2 v)) - 8 \log^3 v \right\}^2 \\ & - \left\{ 225 - 504v^2 + 342v^4 - 72v^6 + 9v^8 + (360 - 288v^2 - 72v^4) \log v \right. \\ & \quad \left. + 144 \log^2 v + (-120 + 96v^2 + 24v^4) \log^3 v - 96 \log^4 v + 16 \log^6 v \right\} \\ & = -144(v^2 - 1)^2 + 144(v^4 - 1) \log v - 48(v^4 - 1) \log^3 v \\ & = 48(v^4 - 1) \left(3 \log v - 3 \left(1 - \frac{2}{v^2 + 1} \right) - \log^3 v \right) \\ & < 0. \end{aligned} \tag{40}$$

Note that this also proves that the expression in the square root in $\zeta_{1,2}$ is positive. Together with $8 \log^3 v < 0$ these inequalities give us $\zeta_2(v) > 1$. These results lead to the conclusion that

$$G_-(v, \zeta) < 0 \iff \zeta \in [0, \zeta_1(v)].$$

The other sign possibilities for G_- follow immediately.

Remark D.1. For the excluded endpoints 0 and 1 we find

$$\begin{aligned} \lim_{v \downarrow 0} \zeta_1 &= 0, & \lim_{v \uparrow 1} \zeta_1 &= \frac{5}{2} - \frac{1}{2} \sqrt{\frac{69}{5}}, \\ \lim_{v \downarrow 0} \zeta_2 &= 1, & \lim_{v \uparrow 1} \zeta_2 &= \frac{5}{2} + \frac{1}{2} \sqrt{\frac{69}{5}}. \end{aligned}$$

The limits for $v \uparrow 1$ were found by calculating the first terms in the Taylor expansion of $\zeta_{1,2}$.

References

- [1] AMBROSETTI, A., MALCHIODI, A., AND NI, W.-M. Solutions, concentrating on spheres, to symmetric singularly perturbed problems. *C. R. Acad. Sci. Paris, Ser. I* 335 (2002), 145–150.
- [2] AMBROSETTI, A., MALCHIODI, A., AND NI, W.-M. Singularly perturbed elliptic equations with symmetry: Existence of solutions concentrating on spheres, part I. *Commun. Math. Phys.* 235 (2003), 427–466.
- [3] AMBROSETTI, A., MALCHIODI, A., AND NI, W.-M. Singularly perturbed elliptic equations with symmetry: Existence of solutions concentrating on spheres, part II. *Indiana University Mathematics Journal* 53, 2 (2004), 297–329.
- [4] AMBROSIO, L., FUSCO, N., AND PALLARA, D. *Functions of Bounded Variation and Free Discontinuity Problems*, first ed. Oxford Mathematical Monographs. Oxford University Press, Oxford, 2000.

- [5] BADIALE, M., AND D'APRILE, T. Concentration around a sphere for a singularly perturbed Schrödinger equation. *Nonlinear Analysis* 49, 49 (2002), 947–985.
- [6] BALDO, S. Minimal interface criterion for phase transitions in mixtures of Cahn-Hilliard fluids. *Ann. Inst. Henri Poincaré* 7, 2 (1990), 67–90.
- [7] BLOM, J. G., AND PELETIER, M. A. A continuum model of lipid bilayers. *European J. Appl. Math.* 15, 4 (2004), 487–508.
- [8] CHOKSI, R., AND REN, X. Diblock copolymer/homopolymer blends: Derivation of a density functional theory. *Physica D* 203 (2005), 100–119.
- [9] CHOKSI, R., AND REN, X. On the derivation of a density functional theory for microphase separation of diblock copolymers. *Journal of Statistical Physics* 113, 1/2 (October 2003), 151–176.
- [10] CHOKSI, R., AND STERNBERG, P. On the first and second variations of a nonlocal isoperimetric problem. *J. reine angew. Math.* 611 (2006), 75–108.
- [11] CROSS, M. C., AND HOHENBERG, P. C. Pattern formation outside of equilibrium. *Rev. Mod. Phys.* 65, 3 (July 1993), 851–1112.
- [12] DAL MASO, G. *An introduction to Γ -convergence*, first ed., vol. 8 of *Progress in Nonlinear Differential Equations and Their Applications*. Birkhäuser, Boston, 1993.
- [13] D'APRILE, T. Behaviour of symmetric solutions of a nonlinear elliptic field equation in the semi-classical limit: Concentration around a circle. *Electronic Journal of Differential Equations* 2000, 69 (2000), 1–40.
- [14] DOELMAN, A., AND VAN DER PLOEG, H. Homoclinic stripe patterns. *SIAM J. Applied Dynamical Systems* 1, 1 (2002), 65–104.
- [15] ESCHER, J., AND MAYER, U. F. Loss of convexity for a modified Mullins-Sekerka model arising in diblock copolymer melts. *Arch. Math.* 77 (2001), 434–448.
- [16] FIFE, P. C., AND KOWALCZYK, M. A class of pattern-forming models. *J. Nonlinear Sci.* 9 (1999), 641–669.
- [17] GENNIP, Y. V., AND PELETIER, M. A. Copolymer-homopolymer blends: global energy minimisation and global energy bounds. *Calc. Var. online first DOI 10.1007/s00526-007-0147-0* (2008).
- [18] GIUSTI, E. *Minimal Surfaces and Functions of Bounded Variation*, first ed., vol. 80 of *Monographs in Mathematics*. Birkhäuser, Boston, 1984.
- [19] HASHIMOTO, T., MITSUMURA, N., YAMAGUCHI, D., TAKENAKA, M., MORITA, H., KAWAKATSU, T., AND DOI, M. Nonequilibrium helical-domain morphology in diblock copolymer melts. *Polymer* 42 (2001), 8477–8481.
- [20] ITO, A. Domain patterns in copolymer-homopolymer mixtures. *Physical Review E* 58, 5 (1998), 6158–6165.
- [21] KINNING, D. J., WINEY, K., AND THOMAS, E. L. Structural transitions from spherical to nonspherical micelles in blends of poly(styrene-butadiene) diblock copolymer and polystyrene homopolymers. *Macromolecules* 21 (1988), 3502–3506.
- [22] KOIZUMI, S., HASEGAWA, H., AND HASHIMOTO, T. Ordered structures of block copolymer/homopolymer mixtures. 5. Interplay of macro- and microphase transitions. *Macromolecules* 27 (1994), 6532–6540.

- [23] LIPOWSKI, R. Vesicles and biomembranes. *Encyclopedia of Applied Physics 23* (1998), 199–222.
- [24] LÖWENHAUPT, B., STEURER, A., HELLMANN, G. P., AND GALLOT, Y. Microphases and macrophases in polymer blends with a diblock copolymer. *Macromolecules 27* (1994), 908–916.
- [25] MALCHIODI, A. Concentration at curves for a singularly perturbed Neumann problem in three-dimensional domains. *GAFSA, Geom. funct. anal. 15* (2005), 1162–1222.
- [26] MALCHIODI, A., AND MONTENEGRO, M. Boundary concentration phenomena for a singularly perturbed elliptic problem. *Communications on Pure and Applied Mathematics LV* (2002), 1507–1568.
- [27] MALCHIODI, A., AND MONTENEGRO, M. Multidimensional boundary-layers for a singularly perturbed neumann problem. *Duke Math. J. 124*, 1 (2004), 105–143.
- [28] MODICA, L., AND MORTOLA, S. Un esempio di γ -convergenza. *Bollettino U.M.I. 5*, 14-B (1977), 285–299.
- [29] MOORE, P. K., AND HORSTHEMKE, W. Localized patterns in homogeneous networks of diffusively coupled reactors. *Physica D 206* (2005), 121–144.
- [30] MURATOV, C. B. Theory of domain patterns in systems with long-range interactions of coulomb type. *Physical Review E 66*, 6 (2002), 066108–1–066108–25.
- [31] NISHIURA, Y., AND OHNISHI, I. Some mathematical aspects of the micro-phase separation in diblock copolymers. *Physica D 84* (1995), 31–39.
- [32] OHTA, T., AND ITO, A. Dynamics of phase separation in copolymer-homopolymer mixtures. *Physical Review E 52*, 5 (1995), 5250–5260.
- [33] OHTA, T., AND NONOMURA, M. Formation of micelles and vesicles in copolymer-homopolymer mixtures. *Progr. Colloid Polym. Sci. 106* (1997), 127–130.
- [34] PELETIER, M. A., AND RÖGER, M. Partial localization, lipid bilayers, and the elastica functional. *Archive for Rational Mechanics and Analysis, online first* (2008).
- [35] REN, X., AND WEI, J. On the multiplicity of solutions of two nonlocal variational problems. *SIAM J. Math. Anal. 31*, 4 (2000), 909–924.
- [36] REN, X., AND WEI, J. Concentrically layered energy equilibria of the diblock copolymer problem. *Euro. Jnl of Applied Mathematics 13* (2002), 479–496.
- [37] REN, X., AND WEI, J. On the spectra of three-dimensional lamellar solutions of the diblock copolymer problem. *SIAM J. Math. Anal. 35*, 1 (2003), 1–32.
- [38] REN, X., AND WEI, J. Triblock copolymer theory: free energy, disordered phase and weak segregation. *Physica D 178* (2003), 103–117.
- [39] REN, X., AND WEI, J. Triblock copolymer theory: Ordered ABC lamellar phase. *J. Non-linear Sci. 13* (2003), 175–208.
- [40] REN, X., AND WEI, J. Wriggled lamellar solutions and their stability in the diblock copolymer problem. *SIAM J. Math. Anal. 37*, 2 (2005), 455–489.
- [41] REN, X., AND WEI, J. Droplet solutions in the diblock copolymer problem with skewed monomer composition. *Calc. Var. 25*, 3 (2006), 333–359.
- [42] REN, X., AND WEI, J. Existence and stability of spherically layered solutions of the diblock copolymer equation. *SIAM J. Appl. Math. 66*, 3 (2006), 1080–1099.

- [43] RÖGER, M., AND TONEGAWA, Y. Convergence of phase-field approximations to the Gibbs-Thomson law. *Calc. Var.* 32 (2008), 111–136.
- [44] SAKAGUCHI, H., AND BRAND, H. R. Stable localized solutions of arbitrary length for the quintic Swift-Hohenberg equation. *Physica D* 97 (1996), 274–285.
- [45] SAKAGUCHI, H., AND BRAND, H. R. Localized patterns for the quintic complex Swift-Hohenberg equation. *Physica D* 117 (1998), 95–105.
- [46] STALIUNAS, K., AND SÁNCHEZ-MORCILLO, V. J. Spatial-localized structures in degenerate optical parametric oscillators. *Physical Review A* 57, 2 (February 1998), 1454–1457.
- [47] STRECKER, K. E., PARTRIDGE, G. B., TRUSCOTT, A. G., AND HULET, R. G. Formation and propagation of matter-wave soliton trains. *Nature* 417 (9 May 2002), 150–153.
- [48] TARANENKO, V. B., STALIUNAS, K., AND WEISS, C. O. Spatial soliton laser: Localized structures in a laser with a saturable absorber in a self-imaging resonator. *Physical Review A* 56, 2 (August 1997), 1582–1592.
- [49] TLIDI, M., MANDEL, P., AND LEFEVER, R. Localized structures and localized patterns in optical bistability. *Physical Review Letters* 73, 5 (1 August 1994), 640–643.
- [50] TSIMRING, L. S., AND ARANSON, I. S. Localized and cellular patterns in a vibrated granular layer. *Physical Review Letters* 79, 2 (14 July 1997), 213–216.
- [51] TZOUKMANIS, N. Near-periodic local minimizers of singularly perturbed functionals with nonlocal term. *SIAM J. Math. Anal.* 37, 5 (2006), 1396–1416.
- [52] UMBANHOWAR, P. B., MELO, F., AND SWINNEY, H. L. Localized excitations in a vertically vibrated granular layer. *Nature* 382 (29 August 1996), 793–796.
- [53] UNEYAMA, T., AND DOI, M. Density functional theory for block copolymer melts and blends. *Macromolecules* 38 (2005), 196–205.
- [54] VAN GENNIP, Y. *Partial localisation in a variational model for diblock copolymer-homopolymer blends*. Ph.D. Thesis Technische Universiteit Eindhoven, 2008. ISBN 978-90-386-1404-5, <http://alexandria.tue.nl/extra2/200811534.pdf>.
- [55] VANAG, V. K., AND EPSTEIN, I. R. Stationary and oscillatory localized patterns, and subcritical bifurcations. *Physical Review Letters* 92, 12 (26 March 2004), 128301–1–128301–4.
- [56] VILLANI, C. *Optimal transport, old and new*, preprint ed. Springer Berlin, Heidelberg, New York, 2008. <http://www.umpa.ens-lyon.fr/~cvillani/Cedrif/B07C.StFlour.pdf>.
- [57] ZHANG, J.-J., JIN, G., AND MA, Y. Wetting-driven structure ordering of a copolymer/homopolymer/nanoparticle mixture in the presence of a modulated potential. *Eur. Phys. J. E* 18 (2005), 359–365.